Crashworthiness in preliminary design

Mean crushing force prediction for closed-section thin-walled metallic structures

Anand, Shreyas; Alderliesten, René; Castro, Saullo G.P.

DOI
10.1016/j.ijimpeng.2024.104946

Publication date
2024

Document Version
Final published version

Published in
International Journal of Impact Engineering

International Journal of Impact Engineering 188 (2024) 104946

Contents lists available at ScienceDirect

International Journal of Impact Engineering

journal homepage: www.elsevier.com/locate/ijimpeng

Crashworthiness in preliminary design: Mean crushing force prediction for closed-section thin-walled metallic structures

Shreyas Anand, René Alderliesten, Saullo G.P. Castro *

TU Delft Faculty of Aerospace Engineering, Kluyverweg 1, Delft, 2629 HS, Zuid Holland, Netherlands

ARTICLE INFO

Keywords:
Axial crushing
Crashworthiness
Metallic tubular structures
Thin walled structures
Preliminary design
Analytical models

ABSTRACT

To design crash structures for disruptive aircraft designs, it is required to have fast and accurate methods that can predict crashworthiness of aircraft structures early in the design phase. Axial crushing is one of the key energy absorbing mechanisms during a crash event. In this study, various analytical models proposed for calculation of mean crushing force for thin-walled tubular structures are compared with a database of numerical and experimental values to ascertain their accuracy. Improvements to some of the models have also been proposed. Finally a generalized model based on the studied and improved analytical models for prediction of mean crushing force for closed section thin-walled tubular structures is introduced. The generalized model demonstrates high accuracy when compared against experimental/numerical dataset as evidenced by a high coefficient of determination (R^2) value of 0.97 and can therefore be used to estimate the mean crushing force for closed-section thin-walled metallic tubular structures with various cross-sectional shapes and crushing modes early in the design phase.

1. Introduction

Aviation was responsible for approximately 12% of the total greenhouse gas emissions from the transportation sector in 2020 [3]. At the current rate, if no improvements are made, carbon emissions from the aviation sector are expected to reach 1.8 gigatonnes per year by 2050 [4]. This figure would constitute 4.2% of the aggregate carbon emissions for 2050 [5]. Therefore, the International Air Transport Association(IATA) proposed a strategy for achieving carbon neutrality by the year 2050 [4]. The proposed strategy consists of 4 components: (a) Sustainable Aviation Fuel (SAF), (b) new technologies, (c) infrastructure/operations, and (d) offsetting/carbon capture. Amongst these components, 13% of the reductions are expected to come from new technologies which include more efficient aircraft designs as well as electric and hydrogen propulsion technologies.

To fulfill the demand for more efficient aircraft, more disruptive configurations have been conceptualized. Prime examples of such designs include the Flying-V and the Airbus Maveric. Oosterom and Vos [6] predict a 22% decrease in fuel burn for some versions of the Flying-V compared to an Airbus A350. However, the Flying-V combines the lifting function of the aircraft (wing) with the load-carrying function (fuselage) into a single wing-fuselage structure, resulting in an ovalized fuselage cross-section which leads to a significant decrease in distance between the cabin floor and the ground ($L_1 > L_2$, Fig. 1). As a consequence of this decrease in the available crushing distance, crashworthiness for such disruptive aircraft configurations becomes more challenging as compared to a conventional aircraft configuration. Therefore, to avoid cost overruns and drastic design changes in the later stages of the design process, it is necessary that crashworthiness is assessed early on in the design phase for such disruptive aircraft configurations.

The main challenges involved with an early crashworthiness assessment are related to the unavailability of high-fidelity models that are compatible with current methods based on implicit or explicit dynamic finite-element analyses. The dependence of such models on more detailed geometry definitions makes high-level structural layout trade-offs difficult to implement and computationally costly. Therefore, we propose the use of reduced-order models that are fast and easy to parameterize, allowing iteration through various structural layout configurations. In our research, it is proposed a low-fidelity model consisting of user elements enriched using analytical equations for the various energy absorbing mechanisms, namely axial crushing, plastic bending, and failure of joints. In this paper, the quasi-static analytical modeling of axial crushing for metallic thin-walled structures is explored in detail. The results from these quasi-static analytical models

* Corresponding author.
E-mail addresses: s.anand@tudelft.nl (S. Anand), r.c.alderliesten@tudelft.nl (R. Alderliesten), s.g.p.castro@tudelft.nl (S.G.P. Castro).
URLs: https://www.tudelft.nl/staff/s.anand/ (S. Anand), https://www.tudelft.nl/staff/r.c.alderliesten/ (R. Alderliesten), https://www.tudelft.nl/staff/s.g.p.castro/ (S.G.P. Castro).

https://doi.org/10.1016/j.ijimpeng.2024.104946
Received 1 December 2023; Received in revised form 18 January 2024; Accepted 3 March 2024
Available online 5 March 2024

Nomenclature

c	Edge length of cross-section in polygonal tubular structures
$2H$	Initial distance between plastic hinges at top and bottom of a basic folding element (Fig. 12, Ref. [1])
κ	Effective crushing length
N_c	Number of corners for a polygonal or star shaped cross-section (Ref. [2])
P_{mean}	Mean crushing force
R	Mean radius of cross-section in circular tubular structures
h	Wall thickness for the metallic structures
M_0	Fully plastic bending moment per unit length
σ_0	Flow stress (MPa)
ε_u	Ultimate strain
θ_e	External angle (Fig. 2, Ref. [2])
θ_i	Internal angle (Fig. 2, Ref. [2])
b	Radius of the toroidal surface
$2\psi_0$	π - central angle of a corner element
α	timelike parameter (Fig. 14)
$\overline{\alpha}$	Switching point parameter
R^2	Coefficient of determination
$\overline{E}$	Average error
θ	Enclosed angle for an angle element
B	Edge length of an angle element
IQR	Inter Quartile Range

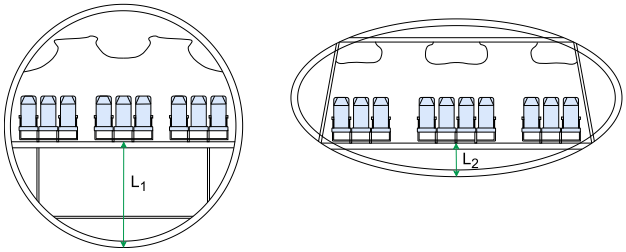

Fig. 1. Comparison between Airbus A350 (left) [7] and Flying-V fuselage cross section (right) [6].

can then be extended to the case of dynamic loading by considering the strain rate effects (Section 5).

To model the axial crushing behavior of metallic thin-walled structures, it is important to be able to predict the force versus displacement curve for a member subjected to axial loads. Metallic structures submitted to axial crushing typically display a progressive folding behavior. An ideal force versus displacement graph for axial crushing of a tubular structure is shown in Fig. 2. When the tubular structure comes into contact with the rigid plane, a force P starts to increase until it reaches a peak (P_{peak}), at this point plastic failure sets in and the crushing transitions into a mechanism of progressive folding corresponding to a mean force (P_{mean}) denoted by a dashed line in Fig. 2.

The prediction of the mean crushing force requires a detailed analysis of the crushing mechanism. Various analytical models have been proposed in the literature for predicting the mean crushing force (P_{mean}) for thin-walled metallic structures submitted to axial crushing. Alexander [8] proposed in 1960 an approximate theory for calculating the mean crushing force for cylindrical thin-walled tubular structures. In

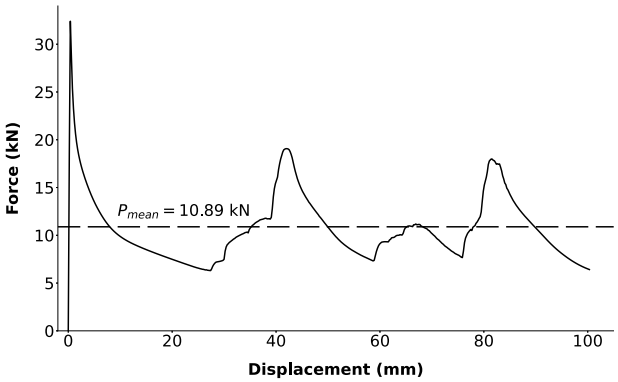

Fig. 2. Ideal force versus displacement curve for a tubular structure.

1978, Magee and Thornton proposed empirical equations for circular and square tubular structures. In the 1980s, Abramowicz et al. proposed a kinematics-based model for square [1], circular [9] and multi-corner [10] tubular structures. Subsequently, in 1992, Wierzbicki et al. [11] revisited Alexander's model and proposed a model using super-folding elements to reproduce the whole crushing process. Singace et al. [12] proposed in 1995 a modification to the eccentricity factor in Weirzbicki's model [11]. In 2007, Liu and Day [13,14] used the methodology from Abramowicz et al. [10] to propose an equation for calculating the mean crushing force for octagonal tubular structures. In 2012, an analytical model for angle elements was proposed by Zhang and Zhang [15]. In 2014, Maalej et al. proposed a closed form solution for calculating P_{mean} for polygonal tubular structures based on the work of Abramowicz et al. [10]. More recently, in 2019, Tabacu et al. [2] proposed a generalized analytical model for polygonal and star-shaped cross-sections based on the membrane energy calculations from Zhang and Zhang [16].

The aforementioned analytical models claimed to correspond well with experimental findings. Therefore, to select the most suitable models for the present study, we decided to evaluate these analytical models against a dataset that includes various materials, geometries, and cross-sections. This dataset includes experimental results compiled from the literature, and simulation results obtained from a shell-based finite element (FE) model.

Four different cross-sectional shapes (circular, square, hexagonal and octagonal) were considered for this study. Square and circular cross-sections are the most commonly studied cross-sections for axial crushing applications. While square tubular structures are better in terms of practicality and ease of manufacturing [17], circular tubular structures have been shown to have better energy absorption characteristics [17–19]. Mamalis et al. [17] note that polygonal tubular structures can lend themselves to easier fabrication while displaying crushing characteristics closer to that of circular tubular structures. It was observed by Yamashita et al. [19] and Fan et al. [20] that for polygonal tubular structures specific energy absorption increases with increase in the number of sides. However, Tarlochan et al. [18] recorded a decrease in specific energy absorption for octagonal tubular structures as compared to hexagonal tubular structures. Yamashita et al. [19] also state that polygonal cross-sections with less than six sides should generally be avoided as they are more susceptible to disordered deformation patterns. Since we want to assess crashworthiness early in the design phase, having the ability to account for different cross-sectional shapes is a significant advantage. Therefore, analytical models for estimating the mean crushing force of circular, square and polygonal tubular structures have been considered in this study.

2. Analytical model parameters

For the considered analytical models, the parameters used for the calculation of the mean crushing force can be divided into two categories: geometrical parameters and material parameters.

Geometrical parameters

1. Wall thickness (h)
2. Side length (c)
3. Mean Radius (R)
4. Number of sides of the polygon/angle enclosed between two edges

Material parameters

1. **Effective crushing length** (κ): Effective crushing length is a key parameter that characterizes the energy absorption capability of a tubular structure during an impact event. For the purposes of this paper, effective crushing length is defined as the proportion of the crushed length to the initial length, with the former being the length of the tubular structure subsequent to full-scale crushing:

$$\text{Effective crushing length, } \kappa = \frac{Crushed\ length}{Initial\ length} \tag{1}$$

2. **Flow stress** (σ_0): Pertaining to the axial crushing of metallic tubular structures, flow stress is the level of stress needed to sustain plastic deformation of the material. The identification of this flow stress is crucial to the calculation of mean crushing force for these metallic structures. Various formulas for calculating flow stress, denoted as σ_0, are available in the published literature:

   (a) Alexander [8]:

$$\sigma_0 = \frac{2}{\sqrt{3}}\sigma_y \tag{2}$$

   (b) Wierzbicki et al. [11]:

$$\sigma_0 = 0.92 \cdot \sigma_u \tag{3}$$

   (c) Wierzbicki et al. [21]:

$$\sigma_0 = 0.70 \cdot \sigma_u \tag{4}$$

   (d) Langseth and Hopperstad [22], Zhang and Zhang [16], Hannsen et al. [23], and Yang and Caldwell [24] use the expression:

$$\sigma_0 = \frac{\sigma_y + \sigma_u}{2} \tag{5}$$

   (e) Tabacu et al. [2]:

$$\sigma_0 = \frac{1}{\varepsilon_u} \cdot \int_0^{\varepsilon_u} \sigma \cdot d\varepsilon \tag{6}$$

3. Analytical models for mean crushing force (P_{mean})

When submitted to axial crushing, metallic tubular structures crush either with an extensional or an inextensional crushing mechanism [1,2]. In extensional crushing mechanism, both sides of a corner element move outwards creating an extension about the edge whereas during inextensional crushing, one side moves outward while the other side moves inward with the material flowing across the edge (plastic hinge line). Both these crushing mechanisms are illustrated in Fig. 3.

Equations proposed by various authors for inextensional and extensional crushing of polygonal tubular structures (concertina crushing for circular tubular structures) are presented in this section. These equations are either obtained by calibration with experimental data [15,25] or by equating mean force times the displacement required for one complete fold with the amount of energy consumed to create the fold (Eq. (7)).

$$P_{mean}.\delta = \text{Energy absorbed for creation of one fold} \tag{7}$$

Where δ is the crushed distance for one complete fold and is generally given by $2H.\kappa$. Energy absorbed for creation of one fold is computed using two different approaches in the presented analytical models. The first approach is more rigorous and considers the finite rotations and deformations that take place during formation of a fold [1,9,10] while the second approach considers the sum of bending and membrane energy required for creation of a fold [2]. For a detailed treatment of energy absorbed in creation of one fold, readers should consult the work of respective authors. However, for completeness one example of the governing equation for each approach is presented below:

1. **Quasi inextensional crushing of polygonal tubular structures per Abramowicz et al.** [10]: The energy required for the creation of one fold is given as a sum of energy absorbed by plastic flow over the toroidal surface (E_1), energy absorbed by bending along the horizontal hinge lines (E_2 and E_5), energy absorbed by bending along the inclined hinge lines (E_3 and E_6), and energy absorbed by stretching of the conical zone (E_4). Energies $E_1 \rightarrow E_6$ are given as functions of fully plastic bending moment (M_0), wavelength of folding ($2H$), radius of toroidal surface (b), side length (c), wall thickness (h), angle of corner element (ψ_0), angle of rotation of sides (α), terminal value of angle of rotation (α_f), switching angle after which the crushing turns extensional ($\bar{\alpha}$) and integrals $I_1 \rightarrow I_6$ (functions of ψ_0 and $\bar{\alpha}$):

$$E_1 = 16M_0\frac{Hb}{h}I_1;\ E_2 + E_5 = 4M_0c\alpha_f;\ E_3 = 4M_0\frac{H^2}{b}I_3;$$
$$E_4 = 8M_0\frac{H^2}{h}I_4 \text{ and } E_6 = 2M_0HI_6 \tag{8}$$

   The equation for mean crushing force (P_mean) is then written as:

$$P_{mean}.2H.\kappa = 16M_0\frac{Hb}{h}I_1 + 4M_0c\alpha_f + 4M_0\frac{H^2}{b}I_3 + 8M_0\frac{H^2}{h}I_4 + 2M_0HI_6 \tag{9}$$

   Eq. (9) can then be further simplified and value of mean crushing force obtained by minimizing with respect to the three unknowns ($\partial P_m/\partial\chi = 0$, where $\chi = [H, b, \bar{\alpha}]$).

2. **Extensional crushing of square tube per Tabacu et al.** [2]: The energy required for creation of one fold is given as a sum of membrane and bending energies. The bending energy is the amount of energy absorbed by bending along the plastic hinge lines while the membrane energy accounts for extension or compression of the material during fold formation. The bending and membrane energies for a corner element can be given as:

$$E_{bending} = 2.\pi.L.M_0 \text{ and } E_{membrane} = 2.\pi.M_0.H^2/h \tag{10}$$

   For a square tubular structure, this leads to:

$$P_{mean}.2H.\kappa = 2.\pi.4c.M_0 + 2.\pi.M_0.\frac{H^2}{h} \tag{11}$$

   The expression for H can then be obtained by putting the partial differential of mean crushing force with H ($\partial P_m/\partial H$) equal to 0 (since the mean crushing force is constant). Final expression of mean crushing force can then be obtained by substituting the expression of H in Eq. (11).

Concertina crushing of circular tubular structures per Alexander (1960) [8]:

$$P_{mean} = K\sigma_0 h^{1.5}\sqrt{2R} \tag{12}$$

where: $K = 6.08$

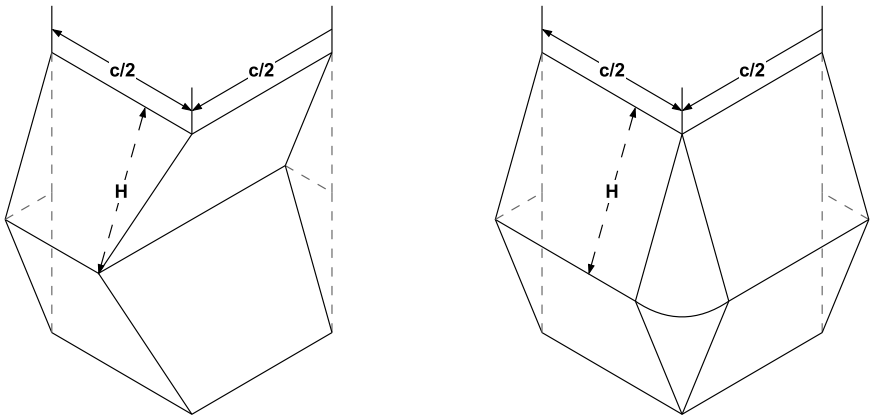

(a) (b)

Fig. 3. Basic collapse elements for (a) Inextensional crushing mechanism and (b) Extensional crushing mechanism.

Concertina crushing of circular tubular structures per Abramowicz et al. (1984) [9]:

$$\frac{P_{\text{mean}}}{M_0}\cdot\kappa = 2\sqrt{3}\pi\left(\frac{R}{h}\right)\left(\frac{H}{R}\right)+\frac{2}{\sqrt{3}}\pi\left(\frac{R}{h}\right)\left(\frac{H}{R}\right)^2+2\pi^2\left(\frac{R}{H}\right)+2\pi \quad (13)$$

where:

$$\frac{H}{R}=\left(\frac{\pi h}{\sqrt{3}R}\left[1+\frac{2}{3}\left(\frac{H}{R}\right)\right]^{-1}\right)^{\frac{1}{2}} \text{ and } M_0=\frac{2\sigma_0 h^2}{4\sqrt{3}}$$

Concertina crushing of circular tubular structures per Wierzbicki et al. (1992) [11]:

$$\frac{P_m}{M_0}=31.74\sqrt{\frac{2R}{h}} \quad (14)$$

where: $M_0=\frac{\sigma_0 h^2}{4}$

Concertina crushing of circular tubular structures per Singace et al. (1995) [12]:

$$\frac{P_m}{M_0}\cdot\kappa = 22.27\sqrt{\frac{2R}{h}}+5.632 \quad (15)$$

where: $M_0=\frac{\sigma_0 h^2}{4}$

Square tubular structures per Magee and Thornton (1978) [25]:

Magee and Thornton obtained an empirical equation for the mean crushing force of square tubular structures:

$$P_m = 17\cdot\sigma_0\cdot c^{0.2}\cdot h^{1.8} \quad (16)$$

Inextensional crushing of square tubular structures per Abramowicz et al. (1984) [1]:

Abramowicz et al. gave an expression for inextensional crushing of square tubular structures:

$$\frac{P_{\text{mean}}}{M_0}\cdot\kappa = 17.76\left(\frac{b}{h}\right)+4\pi\left(\frac{c}{h}\right)\left(\frac{h}{H}\right)+9.184\left(\frac{H}{h}\right)\left(\frac{h}{b}\right) \quad (17)$$

where:

$$\frac{b}{h}=0.72\left(\frac{c}{h}\right)^{\frac{1}{3}};\ \frac{H}{h}=0.99\left(\frac{c}{h}\right)^{\frac{2}{3}} \text{ and } M_0=\frac{\sigma_0 h^2}{4}$$

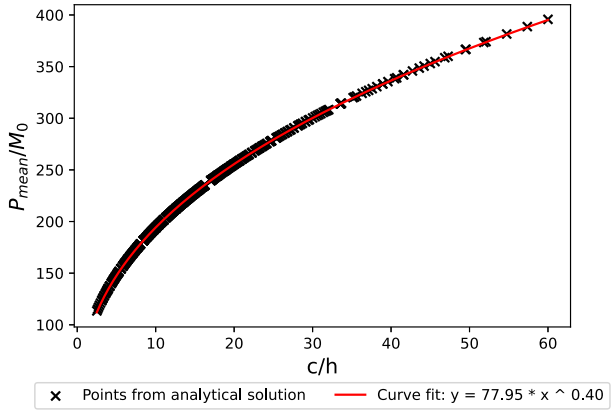

Fig. 4. Fitting a curve to the dataset obtained using the analytical model from Abramowicz et al. [10]).

Quasi inextensional crushing of polygonal tubular structures per Abramowicz et al. (1988, 1989, 1992) [10,26,27]:

$$\frac{P_m\cdot\delta_{eff}}{M_0\cdot 2H}=A_1\frac{b}{h}+(A_2+A_5)\frac{c}{H}+A_3\frac{H}{b}+A_4\frac{H}{h}+A_6 \quad (18)$$

where M_0 is calculated as $\sigma_0 h^2/4$, A_i (i = 1 to 6) is a function of the angle between two edges of a corner element ($\pi - 2\psi_0$) and a time-like parameter (α), b and $2H$ are bending radius and wavelength of the buckling wave respectively. A switching point parameter ($\overline{\alpha}$) is also used in the calculation, the crushing is inextensional below $\overline{\alpha}$ and extensional after $\overline{\alpha}$. The term $\delta_{eff}/2H$ indicates effective crushing length and can be used interchangeably with κ. Since the mean crushing force should remain constant throughout the crushing process, the values of unknowns (b, H, $\overline{\alpha}$) can be obtained by equating the partial differentiation of the mean force with respect to each unknown equal to zero.

For a specific type of cross-section, it is convenient to solve Eq. (18) in terms of the mean crushing force (P_m) for different values of M_0 and c/h. These results will give a set of points in a graph of c/h versus P_m/M_0, for which a simpler curve can be fit, Fig. 4. For the case of mild steel, $\kappa = 0.73$ [10]:

- For hexagonal tubular structures:

$$\frac{P_m}{M_0}=80.92\left(\frac{c}{h}\right)^{0.4} \quad (19)$$

However, in our implementation, we obtain a slightly lower coefficient :

$$\frac{P_m}{M_0} = 77.95\left(\frac{c}{h}\right)^{0.4} \tag{20}$$

The discrepancy in the coefficient value may arise from variations in the selected (c/h) range. Additionally, rounding inaccuracies might also cause a deviation in the value of the coefficient.

- For octagonal tubular structures, following the procedure presented in the paper, we obtain a similar equation:

$$\frac{P_m}{M_0} = 110.24\left(\frac{c}{h}\right)^{0.4} \tag{21}$$

These results are obtained assuming $\kappa = 0.73$, for other kappa values, mean force should therefore be multiplied by $0.73/\kappa$. The same holds true for other models that are based on this model (Eq. (22) and (25)).

Quasi inextensional crushing of polygonal tubular structures per Maalej et al. (2014) [28]:

Maalej et al. [28] used the model from Abramowicz et al. [10] to derive with an empirical closed form solution:

$$\frac{P_m}{M_0} = N_c \cdot (2.13 + 9.44\phi - 2\phi^2)\left(\frac{c}{h}\right)^{\frac{1}{3}+0.06\left(\phi-\frac{\pi}{3}\right)} \tag{22}$$

where:

N_c = Number of corners; ϕ = Corner element angle and $M_0 = \frac{\sigma_0 h^2}{4}$

This equation for specific cases are given below:

- For Hexagonal tubular structures:

$$\frac{P_m}{M_0} = 78.77\left(\frac{c}{h}\right)^{0.4} \tag{23}$$

- For Octagonal tubular structures:

$$\frac{P_m}{M_0} = 106.15\left(\frac{c}{h}\right)^{0.41} \tag{24}$$

Quasi inextensional crushing of octagonal tubular structures per Liu and Day (2007) [13,14]:

$$\frac{P_m}{M_0} = 97.77\left(\frac{c}{h}\right)^{0.4} \tag{25}$$

where: $M_0 = \frac{\sigma_0 h^2}{4}$

This equation is obtained using the model from Abramowicz et al. [10]. However, it is very different from the equation that we obtain in our implementation of Abramowicz et al.'s model (Eq. (21)) and the equation obtained by Maalej et al. [28] (Eq. (22)). During the development of the present study, we were able to identify the source of this deviation, which is a printing error in the work of Abramowicz et al. [10]. The equation for integral I_3 is supposed to be:

$$I_3(\psi_0, \overline{\alpha}) = cot^2\psi_0 \int_0^{\overline{\alpha}} cos\alpha \sqrt{tan^2\psi_0 + sin^2\alpha}\, d\alpha \tag{26}$$

Extensional crushing of polygonal and star-shaped cross sections per Tabacu et al. (2019) [2]:

Tabacu et al. proposed a model for extensional crushing of polygonal and star-shaped cross-sections. The equation for the model from Tabacu et al. [2] takes the form:

$$P_m \cdot \kappa = \sigma_0 \cdot h \cdot N_c \cdot \sqrt{[2\pi - 2(\theta_i + \theta_e)] \cdot \pi \cdot L_e \cdot h} \tag{27}$$

The parameters θ_i, θ_e, L_e and N_c come from the cross-sectional geometry (Fig. 5). The equation for specific cases derived by Tabacu et al. [2] are given below:

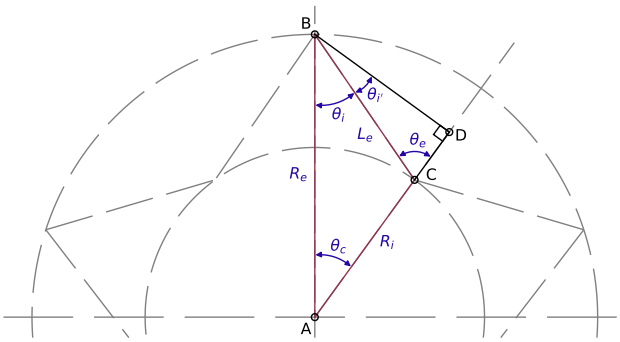

Fig. 5. Geometrical parameters for the model from Tabacu et al. [2].

- For rectangular tubular structures:

$$P_m \cdot \kappa = 8.88 \cdot \sigma_0 \cdot L_e^{\frac{1}{2}} \cdot h^{\frac{3}{2}} \tag{28}$$

- For circular tubular structures:

$$P_m \cdot \kappa = 22.27 \cdot \frac{\sigma_0 \cdot h^2}{4}\sqrt{\frac{2 \cdot R}{h}} \tag{29}$$

- For convex polygon with N_c corners:

Eq. (27) can be further simplified for the case of convex polygons. For convex polygons, $\theta_c = \pi/N_c$ and $\theta_e = \pi/2$. If "c" is the side length of the polygon, then substituting the values of θ_c and θ_e in Eq. (27) result in:

$$P_m \cdot \kappa = \pi \cdot \sigma_0 \cdot N_c^{\frac{1}{2}} \cdot c^{\frac{1}{2}} \cdot h^{\frac{3}{2}} \tag{30}$$

Eq. (30) is very interesting because it indicates that for tubular structures with convex polygonal shapes, the mean crushing force is directly proportional to the square root of the number of sides/corners given by $N_c^{0.5}$. Abramowicz et al. [10] proposed in their work that the inextensional crushing mode is infact a quasi inextensional mode and involves a combination of extensional and inextensional crushing with extensional crushing becoming the dominant mode for obtuse angle elements. Therefore, while the equation from Tabacu et al. [2] specifically deals with extensional crushing, it is also interesting to compare its results with inextensional mean crushing force dataset.

Inextensional crushing of angle elements per Zhang and Zhang (2013) [15]:

Zhang and Zhang proposed a general equation for angle elements with a central angle θ by calibrating a general expression for the mean crushing force with the empirical equation for square tubular structures from Magee and Thornton [25].

$$P_m = \frac{\sigma_0}{2 \cdot \kappa} \cdot (B)^{0.2} \cdot h^{1.8} \cdot \sqrt{\frac{2\pi \cdot tan(\theta/2)}{0.082(tan(\theta/2) + 0.06/tan(\theta/2))}} \tag{31}$$

4. Sensitivity of analytical models to geometrical and material parameters

For the present work, experimental data from literature (Section 6) and numerical simulation data were used to evaluate the accuracy of various analytical models. The analytical models presented in Section 3 use various geometrical and material parameters to estimate the value of the mean crushing force (P_{mean}). which means that an error in the input parameters can lead to a significant error in the estimated value of mean crushing force. Potential sources of error are experimental measurement discrepancies, fabrication inconsistencies, and data reporting approximations.

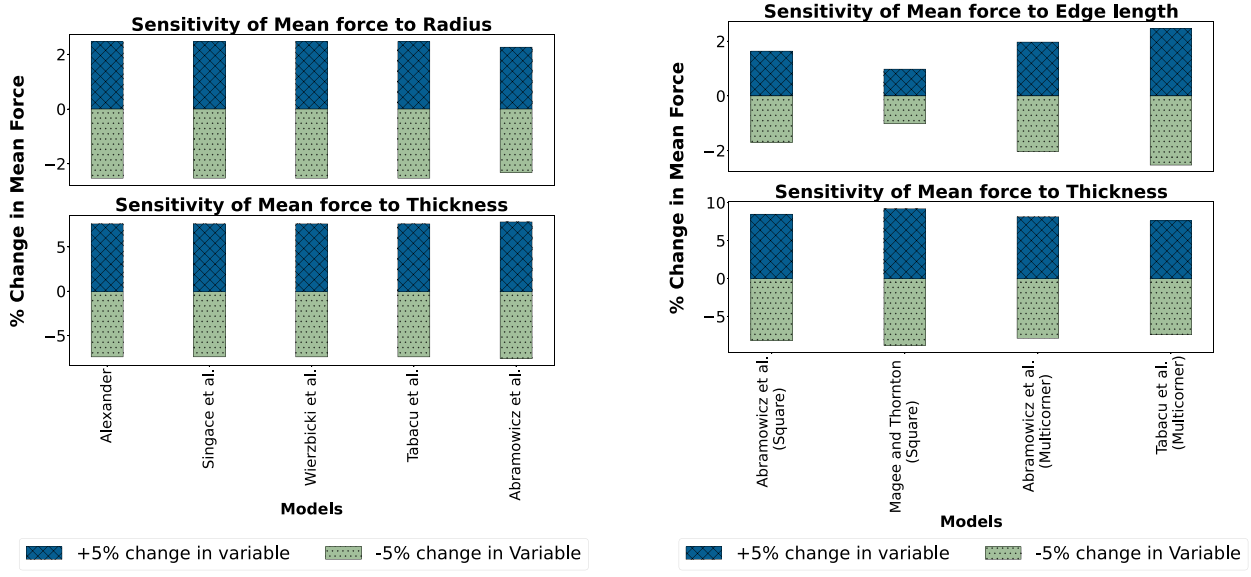

Fig. 6. Sensitivity of analytical models for predicting mean crushing force to radius/ edge length and thickness for (a) circular tubular structures and (b) polygonal tubular structures.

To understand the amount of error that each of the input parameters can cause while estimating the mean crushing force, a sensitivity analysis is conducted for the various models. For all the models, the mean crushing force is directly proportional to the flow stress (σ_0), therefore, a percentage (%) change in flow stress causes the mean force to change by the same percentage.

The sensitivity analyses shown in Figs. 6(a) and 6(b) only investigate the effect of the edge length (radius for circular tubular structures) and thickness. It is evident that the calculations of mean crushing force exhibit a high sensitivity to variations in thickness, meaning that significant errors would be reasonably expected when comparing the analytical models against the experimental dataset obtained from literature, because minor inaccuracies in the reported geometry would result in significant discrepancies in the mean crushing force calculated using the analytical models. Therefore, it becomes imperative for users of these analytical models to remain cognizant of the high sensitivity of such models to thickness variations. Furthermore, since P_{mean} is directly proportional to the flow stress, ensuring high accuracy in the stress–strain data becomes crucial before utilizing these analytical models for comparison against experimental data.

5. Strain rate effects

Since we intend to use the analytical models for impact loading scenarios (aircraft crash), it is essential to adapt results from quasi-static analytical models presented in this paper to take strain rate effects into account. While a detailed study of strain rate effects is outside the scope of this paper, a brief summary of methods from literature which can be used to obtain the dynamic mean crushing force (P_m^d) from the quasi-static mean crushing force (P_m) are presented in this section.

Okhubo et al. [29] proposed an empirical equation (Eq. (32)) by comparing the static and dynamic mean crushing force for closed-hat sections and Wimmer [30] proposed an empirical equation for square box columns (Eq. (33)).

$$P_m^d = P_m\left(1 + 0.0668V\right); \text{ where V is velocity in m s}^{-1} \tag{32}$$

$$P_m^d = P_m\left(1 + 0.07V^{0.82}\right); \text{ where V is velocity in m s}^{-1} \tag{33}$$

Since these methods are empirical and are not suitable for preliminary design, a dynamic correction factor based on viscoplastic analysis was proposed by Akerstorm [31]:

$$P_m^d = P_m\left(1 + 0.11V^{0.714}\right); \text{ where V is velocity in m s}^{-1} \tag{34}$$

Abramowicz et al. [1] proposed to account for strain rate effects using the Cowper–Symonds constitutive relationship which gives dynamic flow stress (σ_0^d) as a function of flow stress (σ_0) and strain rate ($\dot{\epsilon}$).

$$\frac{\sigma_0^d}{\sigma_0} = 1 + \left(\frac{\dot{\epsilon}}{D}\right)^{\frac{1}{p}}; \text{ where D and p are strain-rate parameters for Cowper–Symonds material model} \tag{35}$$

Since mean crushing force (P_m) is directly proportional to flow stress, dynamic mean crushing force (P_m^d) is then obtained by using the following expression:

$$P_m^d = P_m\left[1 + \left(\frac{\dot{\epsilon}}{D}\right)^{\frac{1}{p}}\right] \tag{36}$$

Cowper–Symonds relationship is the most commonly used method [1,9,22,28,32–35] to make a correlation between dynamic mean crushing force (P_m^d) and static mean crushing force (P_m).

6. Experimental and numerical datasets

Section 3 presented various analytical models available in the literature for calculating the mean crushing force for metallic tubular structures. To select an appropriate analytical model to be used in the reduced-order crashworthiness simulation, the output of these models is compared against experimental data from literature, presented in Section 6.1. To augment this dataset, numerical simulations using a shell-based finite element model were also conducted, and the results are presented in Section 6.2. All input files along with the extracted force–displacement results corresponding to the numerical dataset were made available in a public dataset by the authors [36].

6.1. Experimental dataset from literature

The experimental dataset is compiled using data points collected from literature for closed-section thin-walled metallic structures, as detailed below. The dataset for different cross-sections is given in Appendix A, while the corresponding material data in Appendix B.

1. **Circular tubular structures:** 44 data points from 5 sources, consisting of 7 different materials
2. **Square tubular structures:** 42 data points from 6 sources, consisting of 11 different materials
3. **Hexagonal tubular structures:** 9 data points from 4 sources, consisting of 4 different materials
4. **Octagonal tubular structures:** 5 data points from 3 sources, consisting of 3 different materials

6.2. Numerical dataset

At an initial glance, the dataset sourced from the literature appears sufficiently extensive; however, it exhibits certain limitations. Many data points in the collected experimental dataset have the same geometry and material, for example the data from Nia and Hamedani includes 5 square tubular samples made from Al3003-H12 with c = 47.1 mm and h = 1.5 mm. Furthermore, the dataset has few data points for hexagonal and octagonal tubular structures.

Shell based crushing models are frequently used to simulate the crushing response of thin-walled metallic structures and have been shown to be very accurate [2,13,28,37,38]. Therefore, to augment the experimental dataset previously presented, a shell-based finite element model is developed in Abaqus [39], using quadrilateral shell elements with reduced integration (S4R). All models consist of a tubular structure placed between two rigid planes, where a vertical displacement is applied to the top rigid plane, while the bottom plane is encastred and the nodes at the bottom of the tubular structure were connected to the bottom rigid plane.

To induce a more controlled and progressive failure, two types of triggers have been used based on the literature [2,15,38]. For inextensional crushing mode, an indentation trigger is introduced on alternate faces (type-I trigger) whereas an indentation trigger is introduced on all the faces to trigger the extensional crushing mode (type-II trigger). A trigger mechanism initiates the structure into a progressive folding sequence by creating local weakness, ensuring a stable crushing zone and preventing other failure modes like global bending which can lead to a significantly lower energy absorption [18,40,41]. Employing a trigger mechanism also results in a reduction of peak crushing force which is especially desirable for crash applications as the human body is susceptible to severe injury when exposed to high deceleration magnitude and onset rates [42]. Trigger mechanisms have been evaluated for a variety of applications including automotive crash box [18,40], helicopter structures [43], and landing gear [44].

Finally, to obtain the force versus displacement curves (cf. Fig. 2), a reference node is placed at the center of the top rigid plane where both the reaction force and the displacement are measured. The numerical dataset is presented in Appendix C. Fig. 7 illustrates a finite element model used for hexagonal tubular structures. The numerical simulation campaign consisted of:

1. **Circular tubular structures:** 32 simulations with 2 different materials (20 simulations using AA6060-T4 and 12 simulations using AISI-316). For AA6060-T4, the combinations considered were composed of Radius, R (mm) = [15, 20, 25, 30] and thickness, h (mm) = [1, 1.25, 1.5, 1.75, 2]. For AISI-316, the combinations considered were composed of Radius, R (mm) = [15, 20, 25, 30] and thickness, t (mm) = [1, 1.25, 1.5]. All the simulations are triggered for an extensional crushing mode as all the models for circular tubular structures presented in this paper deal with this mode of crushing.
2. **Square tubular structures:** 40 simulations with 2 different materials (28 simulations using AA6060-T4 and 12 simulations using AISI-316). For AA6060-T4, the combinations considered were composed of Side length, c (mm) = [30, 40, 50, 60] and thickness, h (mm) = [1, 1.25, 1.5, 1.75, 2, 2.25, 2.5]. For AISI-316, the combinations considered were composed of Side length, c (mm) = [30, 40, 50, 60] and thickness, t (mm) = [1, 1.25, 1.5]. All the simulations are triggered for an inextensional crushing mode as this mode is predominant in the crushing of square tubular structures.

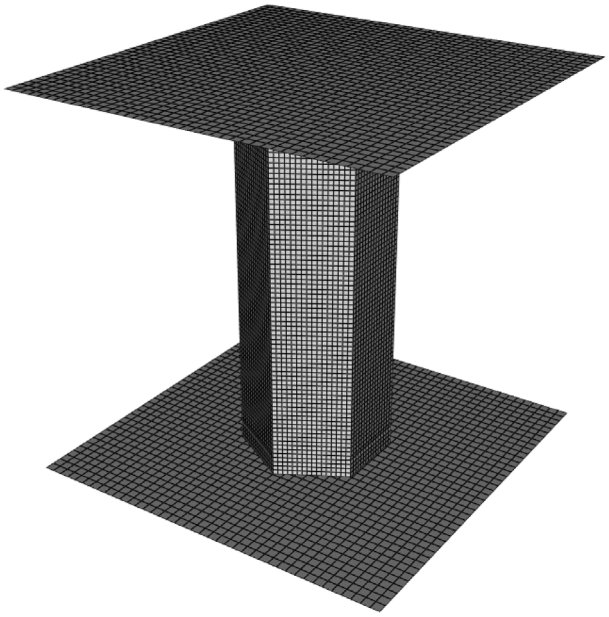

Fig. 7. Numerical model for a hexagonal tubular structure.

3. **Hexagonal tubular structures:**
   Extensional crushing simulations
   20 simulations with 2 different materials (12 simulations using AA6060-T4 and 8 simulations using AISI-316). For AA6060-T4, the combinations considered were composed of Side length, c (mm) = [30, 40, 50, 60] and thickness, h (mm) = [1, 1.5, 2]. For AISI-316, the combinations considered were composed of Side length, c (mm) = [30, 40, 50, 60] and thickness, t (mm) = [1, 1.5].
   Inextensional crushing simulations
   40 simulations with 2 different materials (20 simulations using AA6060-T4 and 20 simulations using AISI-316). For AA6060-T4, the combinations considered were composed of Side length, c (mm) = [30, 40, 50, 60] and thickness, h (mm) = [1, 1.25, 1.5, 1.75, 2]. For AISI-316, the combinations considered were composed of Side length, c (mm) = [30, 40, 50, 60] and thickness, t (mm) = [1, 1.12, 1.25, 1.37, 1.5].
4. **Octagonal tubular structures**
   Extensional crushing simulations
   20 simulations with 2 different materials (12 simulations using AA6060-T4 and 8 simulations using AISI-316). For AA6060-T4, the combinations considered were composed of Side length, c (mm) = [30, 40, 50, 60] and thickness, h (mm) = [1, 1.5, 2]. For AISI-316, the combinations considered were composed of Side length, c (mm) =[30, 40, 50, 60] and thickness, t (mm)= [1, 1.5].
   Inextensional crushing simulations
   A total of 40 simulations were launched with 2 different materials (20 simulations using AA6060-T4 and 20 simulations using AISI-316) and type-I (inextensional) trigger. However, it was observed that tubular structures with $c/h \leq 30$ have a tendency to crush under extensional or mixed crushing mode even when type-I trigger (Inextensional trigger) is used. Therefore, only 26 tubes that crushed with an inextensional crushing mode are considered. For AA6060-T4, the combinations considered were composed of Side length, c (mm) = [30, 40, 50, 60] and

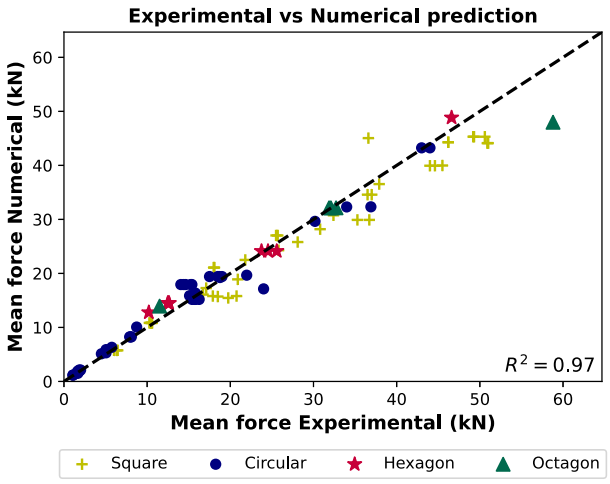

Fig. 8. Correlation between experimental dataset and results from numerical model.

thickness, h (mm) = [1, 1.25, 1.5, 1.75, 2]. For AISI-316, the combinations considered were composed of Side length, c (mm) = [30, 40, 50, 60] and thickness, t (mm) = [1, 1.12, 1.25, 1.37, 1.5].

6.3. Validation of numerical model

To validate the numerical shell model, datapoints from the collected experimental dataset were simulated using the numerical model and a comparison was made. Material data for the respective experimental datapoints was obtained by digitizing the published stress–strain curves. The results obtained show a very good correlation between numerical and experimental data, as evidenced by a high coefficient of correlation (R^2 = 0.97), reinforcing the ability of numerical model to simulate axial crushing of metallic tubular structures. The correlation between experimental dataset and obtained numerical results is presented in Fig. 8.

7. Results

The accuracy of various analytical models is evaluated comparing the mean crushing force predictions against the combined dataset including the experimental data from literature and numerical simulations. The following sub-sections present these comparisons for varying cross-sectional shapes.

For the models presented in this work, different equations to compute flow stress have been proposed by the respective authors. However, since we want to use these analytical models to study crashworthiness early in the design phase, it is important that the considered models can be used for different metallic materials and therefore, calculating flow stress solely based on yield and ultimate stress values will not be appropriate. To ensure that the comparison between analytical models is relevant for different materials, flow stress for all the models presented in this section has been calculated using Eq. (6) which considers the entire stress–strain curve for computation of flow stress. It was also observed by Abramowicz et al. [45] that flow stress obtained using Eq. (6) can be used for theoretical predictions over a wider range of materials.

7.1. Extensional crushing of circular tubular structures

Figs. 9(a) to 9(e) show the comparisons for circular tubular structures. The model from Alexander (Eq. (12)) underpredicts significantly, reaching R^2 = 0.73. A very good agreement is observed for the model from Abramowicz et al. (Eq. (13)), R^2 = 0.98. The revisited Alexander's model from Wierzbicki et al. (Eq. (14)) and the subsequent revisit of Weirzbicki from Singace et al. (Eq. (15)) also show good agreement with the dataset, reaching R^2 = 0.95 and R^2 = 0.94 respectively for these two cases. Finally, for the model from Tabacu et al. (Eq. (29)), a slight under-prediction is observed, with R^2 = 0.91. The reason for the underestimation of mean crushing force using the equation from Tabacu et al. (29) is discussed further in Section 9.

7.2. Inextensional crushing of square tubular structures

As shown in Fig. 10(a), for square tubular structures the model from Magee and Thornton (Eq. (16)) slightly underpredicts the mean crushing force. Fig. 10(b) presents the comparison based on the model from Abramowicz et al. (Eq. (17)), a good correlation fit is observed between the model and the dataset, with R^2 = 0.95. Finally, the extensional crushing model from Tabacu et al. (Eq. (28)) overpredicts the inextensional mean force by a large margin, reaching R^2 = 0.59, the comparison is presented in Fig. 10(c).

7.3. Inextensional crushing of hexagonal tubular structures

For hexagonal tubular structures, the model from Abramowicz et al. (Eq. (19)) for multi-corner sheet metal columns, the model from Zhang and Zhang (Eq. (31)) for angle elements, and the model from Tabacu et al. (Eq. (30)), are used in the comparison. The model from Zhang and Zhang shows reasonable agreement with the inextensional mean crushing force dataset (R^2 = 0.86), however, the model from Abramowicz et al. overpredicts the mean crushing force by a very large margin (R^2 = −0.29). The results obtained are presented in Figs. 11(a) and 11(b).

Interestingly, the extensional crushing model from Tabacu et al. also shows reasonable agreement with the inextensional mean crushing force dataset (R^2 = 0.86), which seems to be in line with Abramowicz et al.'s observation that the extensional crushing becomes the dominant mode for quasi inextensional crushing of obtuse angle elements (Fig. 11(c)).

7.4. Inextensional crushing of octagonal tubular structures

Again, the models from Abramowicz et al. (Eq. (21)), the model from Zhang and Zhang (Eq. (31)) for angle elements and the model from Tabacu et al. (Eq. (30)) are compared against experimental/numerical database. As in the case of hexagonal tubular structures, the model from Abramowicz et al. significantly overestimates the mean crushing force (R^2 = −0.41). The model from Zhang and Zhang also over-predicts the mean crushing force, although by a much smaller margin as compared to the model from Abramowicz et al. (R^2 = 0.90). The results for these two cases are presented in Figs. 12(a) and 12(b).

The extensional crushing model from Tabacu et al. also shows very good agreement with inextensional mean crushing force dataset for octagonal tubular structures (Fig. 12(c)), with R^2 of 0.98.

7.5. Extensional crushing of hexagonal and octagonal tubular structures

The dataset for extensional crushing for hexagonal and octagonal tubular structures was compared against the model from Stefan et al. (Eq. (30)). The results are presented in Figs. 13(a) and 13(b), for both the cases the model from Tabacu et al. was shown to have a good accuracy with an R^2 of 0.99 for hexagonal tubular structures and an R^2 of 0.93 for octagonal tubular structures.

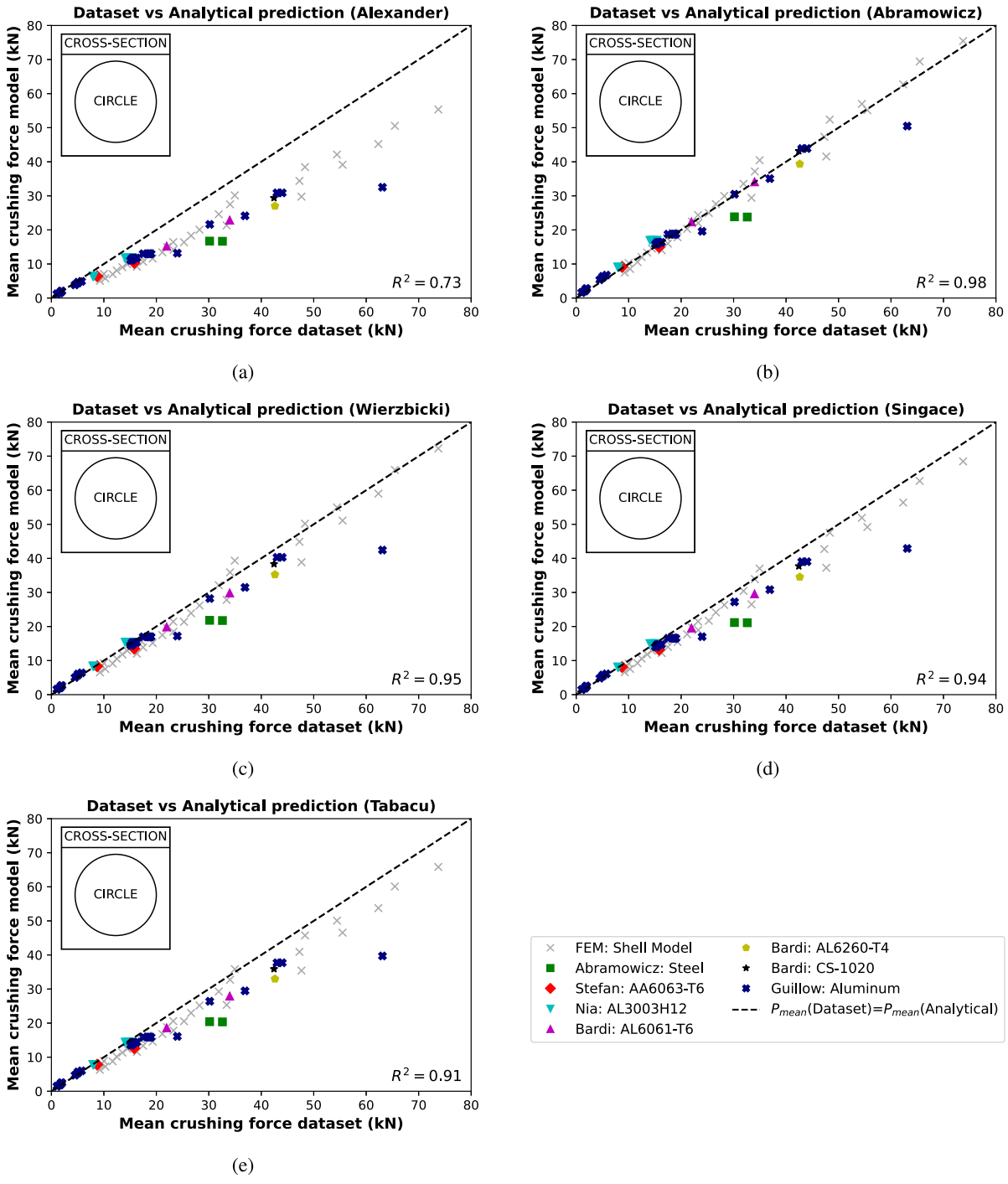

Fig. 9. Comparison between analytical models and dataset for circular tubular structures: (a) Alexander [8], (b) Abramowicz et al. [9], (c) Wierzbicki et al. [11], (d) Singace et al. [12] and (e) Tabacu et al. [2].

8. Modification to the model from abramowicz et al. [10]

As seen in Section 7, the superfolding element model from Abramowicz et al. over-predicts by a very large margin for both hexagonal and octagonal tubular structures. In this section, we propose a slightly altered set of equations to better estimate the mean crushing force. The main equation for the model remains the same (Eq. (18)):

$$\frac{P_m \cdot \delta_{eff}}{M_0 \cdot 2H} = A_1 \frac{b}{h} + (A_2 + A_5)\frac{c}{H} + A_3 \frac{H}{b} + A_4 \frac{H}{h} + A_6 \tag{37}$$

where: $A_1 = 8 \cdot I_1(\psi_0, \overline{\alpha})$ $A_2 + A_5 = 2 \cdot \alpha_f$, where $\alpha_f = \frac{\pi}{2}$

$A_3 = 2 \cdot I_3(\psi_0, \overline{\alpha})$

$A_4 = 4 \cdot I_4(\psi_0, \overline{\alpha})$

$A_6 = I_6(\psi_0, \overline{\alpha})$

Integral $I_1(\psi_0, \overline{\alpha})$ comes from Weirzbicki and Abramowicz [46], the limits are changed from $(0 \to \pi/2)$ to $(0 \to \overline{\alpha})$:

$$I_1(\alpha_m, \psi_0) = \frac{\pi}{\pi - 2\psi_0} \int_0^{\overline{\alpha}} \cos(\alpha) \left\{ \sin(\psi_0) \sin\left(\frac{\pi - 2\psi_0}{\pi}\beta\right) + \cos(\psi_0)\left[1 - \cos\left(\frac{\pi - 2\psi_0}{\pi}\beta\right)\right]\right\} d\alpha \tag{38}$$

where: $\beta = tan^{-1}\left\{\frac{tan(\alpha)}{sin(\psi_0)}\right\}$

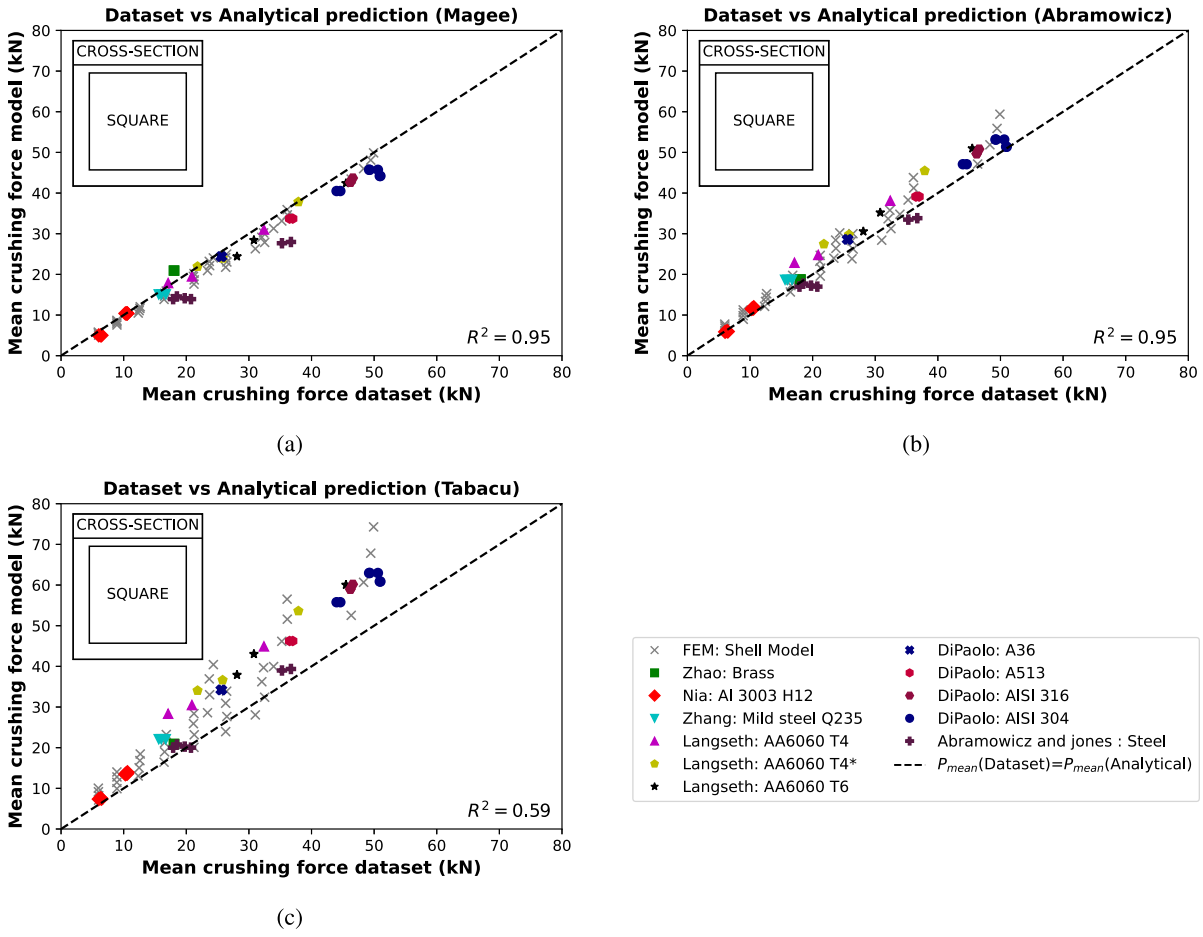

Fig. 10. Comparison between analytical models and dataset for square tubular structures: (a) Magee and Thornton [25], (b) Abramowicz et al. [1] and (c) Tabacu et al. [2].

Integral I_3 in the original model is calculated by multiplying the rate of rotation $\dot{\omega}$ with the length of the inclined hinge line $l = 2H/sin(\gamma)$, where γ is related to α and ψ_0 by the relation:.

$$\gamma = tan^{-1}\left\{\frac{tan(\psi_0)}{sin(\alpha)}\right\} \tag{39}$$

The term $\dot{\omega}$ is related to the tangential velocity (V_t) and radius of toroid (b) as:

$$\dot{\omega} = \frac{V_t}{b} \tag{40}$$

where V_t is computed as the rate of change of length of line BD (Fig. 14), and is given by the expression:

$$V_t = \frac{H \cdot cos(\alpha)}{tan(\psi_0)} \cdot \dot{\alpha} \tag{41}$$

Subsequently the equation for the rate of change of energy, $\dot{E}_3$ is obtained by substituting the values of l and $\dot{\omega}$ into the equation:

$$\dot{E}_3 = 2 \cdot M_0 \cdot l \cdot \dot{\omega} = \frac{4 \cdot M_0 \cdot H^2 \cdot cos(\alpha)}{b \cdot sin(\gamma) \cdot tan(\psi_0)} \cdot \dot{\alpha} \tag{42}$$

However, it is interesting to note here that the velocity is assumed to be constant all along the inclined hinge lines. Instead of making this assumption, it is possible to express the rate of energy in terms of the rate of change of area of the triangles LBD and OBD (Fig. 14).

$$\dot{E}_3 = 2 \cdot M_0 \cdot \frac{dS}{b} \tag{43}$$

Since the length of LD and OD remain constant, dS can be expressed in terms of the rate of change of BD, which leads to the expression:

$$\dot{E}_3 = \frac{2 \cdot M_0 \cdot H^2 \cdot cos(\alpha)}{b \cdot tan(\psi_0)} \cdot d\alpha \tag{44}$$

and E_3 can then be written as:

$$E_3 = \frac{4 \cdot M_0 \cdot H^2}{b} \cdot I_3(\psi_0, \overline{\alpha}) \tag{45}$$

where integral I_3 is:

$$I_3(\psi_0, \overline{\alpha}) = \frac{1}{2}\int_0^{\overline{\alpha}} \frac{cos(\alpha)}{tan(\psi_0)} \cdot d\alpha \tag{46}$$

The expressions for integrals I_4 and I_6 remain the same as in the work of Abramowicz et al. [10]:

$$I_4(\psi_0, \overline{\alpha}) = \int_{\overline{\alpha}}^{\alpha_f} \frac{sin\overline{\alpha} \cdot tan\psi_0 \cdot sin2\alpha}{2(sin^2\overline{\alpha} + tan^2\psi_0 sin^2\alpha)} \cdot d\alpha + \int_{\overline{\alpha}}^{\alpha_f} \left[tan^{-1}\left(\frac{sin\alpha \cdot tan\psi_0}{sin\overline{\alpha}}\right) - \psi_0\right] cos\alpha \cdot d\alpha \tag{47}$$

$$I_6(\psi_0, \overline{\alpha}) = \frac{2}{tan\psi_0}\int_{\overline{\alpha}}^{\alpha_f} \frac{sin\overline{\alpha}(sin^2\overline{\alpha} + tan^2\psi_0)}{sin^2\overline{\alpha} + tan^2\psi_0 sin^2\alpha} \cdot d\alpha \tag{48}$$

Using the integrals above and following the procedure presented by Abramowicz et al. [10], we obtained the following equations for Hexagonal and Octagonal tubular structures:

$$\text{Hexagon}: \frac{P_m}{M_0} \cdot \kappa = 50.72\left(\frac{c}{h}\right)^{0.36} \tag{49}$$

$$\text{Octagon}: \frac{P_m}{M_0} \cdot \kappa = 71.43\left(\frac{c}{h}\right)^{0.36} \tag{50}$$

Eqs. (49) and (50) result in a significant decrease in over-prediction. The new equation results in much more reasonable predictions of mean crushing force for hexagonal tubular structures (Fig. 15(a)). However, the model still significantly overestimates the mean crushing force for octagonal tubular structures (Fig. 15(b)).

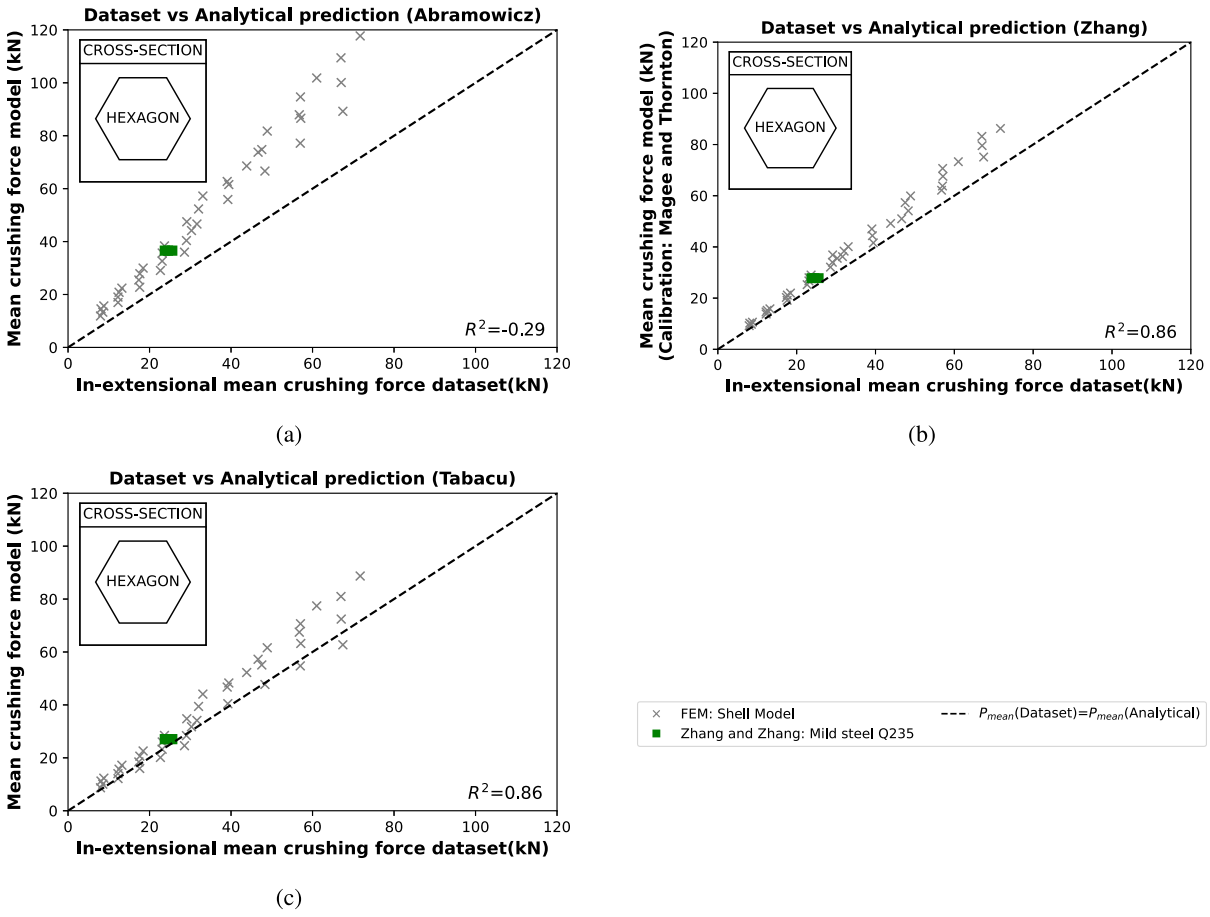

Fig. 11. Comparison between analytical models and dataset for hexagonal tubular structures: (a) Abramowicz et al. [10], (b) Zhang and Zhang [15] and (c) Tabacu et al. [2].

9. Tabacu et al.'s model [2] for circular structures

For the purposes of the present work, the model from Tabacu et al. is very desirable due to its ability to handle various types of cross-sectional shapes. However, we observed an under-prediction for the case of circular tubular structures, a slight modification which improves the prediction is presented in this section.

For circular tubular structures, Tabacu et al. [2] propose using Eq. (27) with a high value of N_c ($N_c \approx 999$) which leads to Eq. (29). From the results presented in Fig. 9(e), we can observe that Eq. (29) slightly underpredicts the mean crushing force. Tabacu et al. derive the equation for mean crushing force using $\sigma_0 \cdot h^2/4$ as the value of fully plastic bending moment, M_0. While the value of $\sigma_0 \cdot h^2/4$ can be used for polygonal tubular structures, this value is not well suited for circular tubular structures because the geometry of circular tubular structures can be considered as an infinitely wide beam which leads to largely plane strain and incompressible conditions, as observed by Alexander [8]. Under such conditions, if Von-Mises criterion is used the stress will be raised to $2/\sqrt{3}\sigma_0$ and subsequently M_0 is given by the equation:

$$M_0 = \frac{2}{\sqrt{3}} \cdot \frac{\sigma_0 \cdot h^2}{4} \tag{51}$$

Taking this value of M_0 into account, and following the procedure presented by Tabacu et al. [2], the bending energy takes the form:

$$E_b = 4\pi^2 R M_0 \tag{52}$$

while the membrane energy takes the form:

$$E_m = \frac{4\sqrt{3}\pi H^2 M_0}{h} \tag{53}$$

The mean force is then given by the equation:

$$\frac{P_m}{M_0} \cdot \kappa = \frac{2\pi^2 R}{H} + \frac{2\sqrt{3}\pi H}{h} \tag{54}$$

Finally, minimizing with respect to H to obtain the value of H and then substituting it back into Eq. (54), we obtain the equation for mean force:

$$P_m \cdot \kappa = \frac{2 \cdot \sigma_0 \cdot \pi^{\frac{3}{2}} \cdot h^{\frac{3}{2}} R^{\frac{1}{2}}}{3^{\frac{1}{4}}} \tag{55}$$

Eq. (55) led to an improvement in the correlation between the analytically obtained mean crushing force and the dataset, as illustrated in Fig. 16, where R^2 increases from 0.91 to 0.94.

10. Calibration of Zhang and Zhang's model [15] with our dataset

In their work Zhang and Zhang [15,16] gave a general expression of the inextensional membrane energy for a corner element with enclosed angle θ and corner element edge length B:

$$E_m(\theta) = \frac{2 \cdot M_0 \cdot H^2 \cdot tan\left(\frac{\theta}{2}\right)}{0.082 \cdot h \cdot \left(\frac{B}{h}\right)^{0.6} \cdot \left(tan\left(\frac{\theta}{2}\right) + \frac{0.06}{tan\left(\frac{\theta}{2}\right)}\right)} \tag{56}$$

Eq. (56) for membrane energy is derived by assuming an equation for rolling radius, P_{mean} for an angle element is then expressed in the form:

$$P_m = \frac{\sigma_0}{2 \cdot \kappa} \cdot (B)^{0.5} \cdot h^2 \cdot \sqrt{\frac{2\pi \cdot tan(\theta/2)}{a_1 \cdot B^{a_2} \cdot h^{1-a_2}(tan(\theta/2) + a_3/tan(\theta/2))}} \tag{57}$$

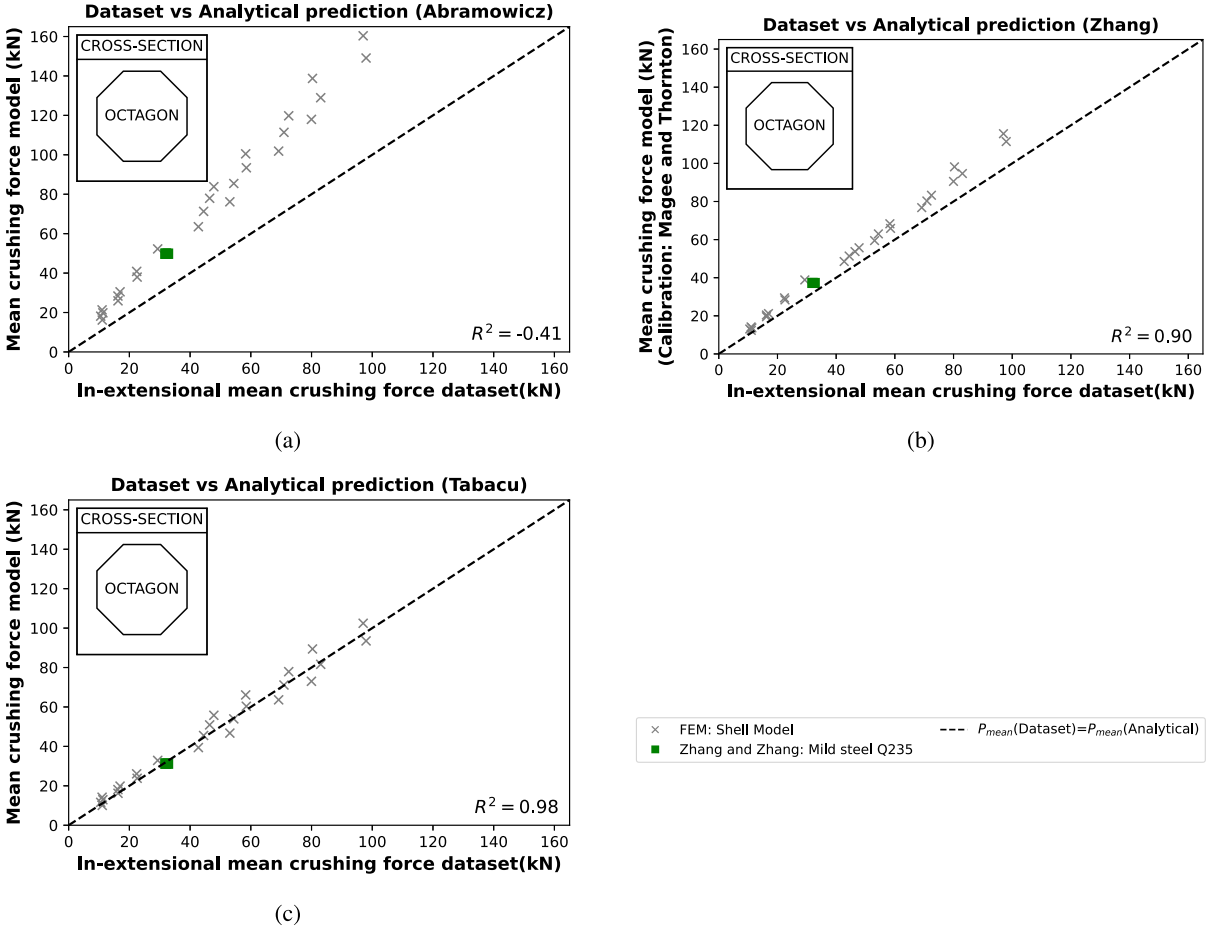

Fig. 12. Comparison between analytical models and dataset for octagonal tubular structures: (a) Abramowicz et al. [10], (b) Zhang and Zhang [15] and (c) Tabacu et al. [2].

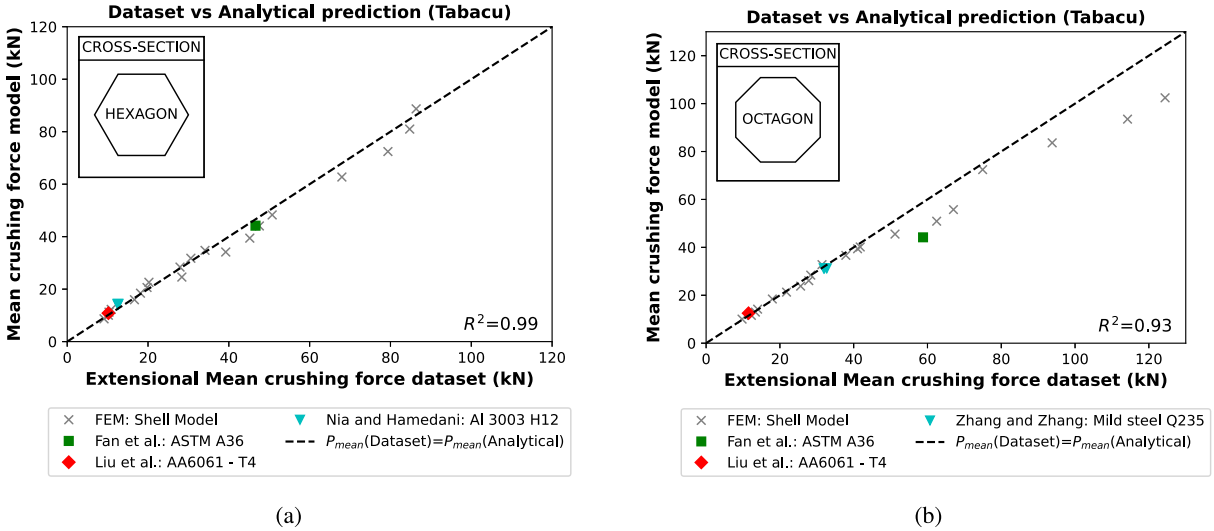

Fig. 13. Comparison between analytical model from Tabacu et al. [2] and extensional mean crushing force dataset for (a) Hexagonal tubular structures and (b) Octagonal tubular structures.

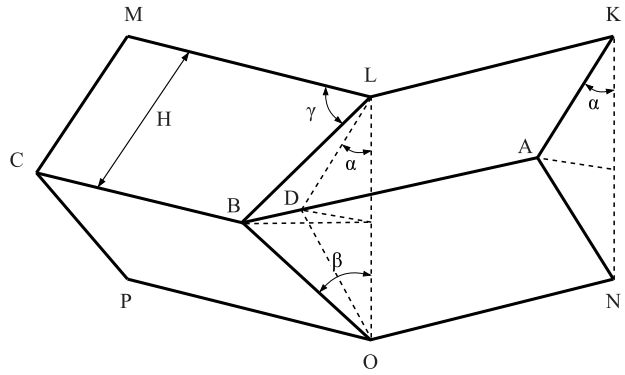

Fig. 14. Superfolding element proposed by Abramowicz et al. [10] (Phase-I)

The unknowns of Eq. (57) are then calculated by calibrating Eq. (57) to be equivalent to a quarter of Eq. (16), from Magee and Thornton [25] for square tubular structures:

$$P_m = \frac{\sigma_0}{2 \cdot \kappa} \cdot (B)^{0.2} \cdot h^{1.8} \cdot \sqrt{\frac{2\pi \cdot tan(\theta/2)}{0.082(tan(\theta/2) + 0.06/tan(\theta/2))}} \tag{58}$$

In the course of our investigation, we determined that, for $\theta = 90°$ and $\kappa = 0.73$, the value of a_1 must be 0.116 to ensure equivalence between Eqs. (16) and (58). Nevertheless, as the precise methodology used to determine $a_1 = 0.082$ has not been detailed, we kept the value $a_1 = 0.082$ for subsequent calculations. Putting $\theta = \pi/2$ in Eq. (58), replacing B with $c/2$, where c is the edge length of the square tubular structure and multiplying by $N_c = 4$, we get:

$$P_m = \frac{14.80}{\kappa} \cdot \sigma_0 \cdot c^{0.2} \cdot h^{1.8} \tag{59}$$

Since the procedure followed by Tabacu et al. and Zhang and Zhang are identical, substituting the expression for the inextensional membrane energy (56) in place of the extensional membrane energy in the model from Tabacu et al. will also lead to Eq. (59). Using this equation from Zhang and Zhang, results in a good fit with experimental/numerical data with an R^2 of 0.96. The results using Eq. (59) are presented in Fig. 17.

As mentioned in sub- Section 7.2, the empirical model from Magee and Thornton [25] slightly underpredicts the mean crushing force for our dataset. The empirical relation by Magee and Thornton was obtained by fitting a power law to the experimental data. Since our dataset is larger than the one used by Magee and Thornton, it is interesting to obtain an empirical equation based on our dataset. The following expression, relating the mean crushing force to the c/h ratio, is utilized for the curve fitting:

$$\frac{P_m}{M_0} \cdot \kappa = a \cdot \left(\frac{c}{h}\right)^b \tag{60}$$

Assuming a constant effective crushing length of $\kappa = 0.73$, the equation from Magee and Thornton can also be transformed to a similar form:

$$\frac{P_m}{M_0} \cdot \kappa = 49.64 \cdot \left(\frac{c}{h}\right)^{0.2} \tag{61}$$

Fig. 18 illustrates the curve fit obtained for our dataset, the equation from Magee and Thornton is also plotted for comparison. From the curve fitting, the parameters a and b were determined to be 65.73 and 0.15 respectively, which indicates a lesser sensitivity of the mean crushing force to the edge length for a square tubular structure.

Rewriting Eq. (60) based on the obtained values of a and b:

$$\frac{P_m}{M_0} \cdot \kappa = 65.73 \cdot \left(\frac{c}{h}\right)^{0.15} \tag{62}$$

It is also of interest to use this new expression of Eq. (62) to calibrate the model from Zhang and Zhang (Eq. (57)), aiming to obtain an expression for inextensional crushing of angle elements. Following the procedure given by Zhang and Zhang [15], the following equation for an angle element is obtained:

$$P_m = \frac{\sigma_0}{2\kappa} \cdot B^{0.15} \cdot h^{1.85} \cdot \sqrt{\frac{2\pi \cdot tan(\theta/2)}{0.071(tan(\theta/2) + 0.06/tan(\theta/2))}} \tag{63}$$

Using the material data from [38], a value of 146 MPa for σ_0 is obtained using Eq. (6). Fig. 15 presents a comparison between the numerical results from Zhang and Zhang (Table 1 in [15]) with the results obtained using Eq. (63). For comparison, the results obtained using Eq. (59) are also plotted, for this equation $\sigma_0 = 106$ MPa is retained from the original work. After calibration with our dataset, an even better correlation is observed between the numerical and analytical values, with R^2 increasing from 0.987 for calibration using Magee and Thornton's dataset to 0.989 for calibration using our dataset. The R^2 value, when only considering elements with $\theta = 90°$, also increases from 0.986 to 0.995 (see Fig. 19).

Further, this new expression based on Zhang and Zhang's model (63) can be used to estimate the mean crushing force for inextensional crushing of hexagonal and octagonal tubular structures (Figs. 20(a) and 20(b)). For hexagonal tubular structures, the R^2 value increased from 0.86 to 0.95 and for the octagonal tubular structures, the R^2 value increased from 0.90 to 0.97.

11. Generalized mean crushing force expression for axial crushing of metallic tubular structures

Based on the results presented in the previous sections, we find that the following models demonstrate a good agreement with the experimental/numerical mean crushing force dataset and can also be rewritten in a simpler form:

1. Model from Tabacu et al. with modified M_0 for circular tubular structures, further simplifying Eq. (55):

$$\frac{P_m}{M_0} \cdot \kappa = 33.85 \cdot N_c^0 \cdot \left(\frac{R}{h}\right)^{0.5} \tag{64}$$

   The N_c term is added to maintain similarity with the other two models presented in this section.
2. Model from Tabacu et al. for extensional crushing of polygonal tubular structures, further simplifying Eq. (30):

$$\frac{P_m}{M_0} \cdot \kappa = 12.56 \cdot N_c^{0.5} \cdot \left(\frac{c}{h}\right)^{0.5} \tag{65}$$

3. Model from Zhang and Zhang for inextensional crushing of polygonal tubular structures calibrated to our dataset (Eq. (63)):

$$P_m = \frac{N_c \cdot \sigma_0}{2\kappa} \cdot B^{0.15} \cdot h^{1.85} \cdot \sqrt{\frac{2\pi \cdot tan(\theta/2)}{0.071(tan(\theta/2) + 0.06/tan(\theta/2))}} \tag{66}$$

   Putting $B = c/2$, moving M_0 to the left side of the equation and further simplifying:

$$\frac{P_m}{M_0} \cdot \kappa = 16.93 \left(\frac{c}{h}\right)^{0.15} \cdot \sqrt{\frac{N_c^2 \cdot tan(\theta/2)}{(tan(\theta/2) + 0.06/tan(\theta/2))}} \tag{67}$$

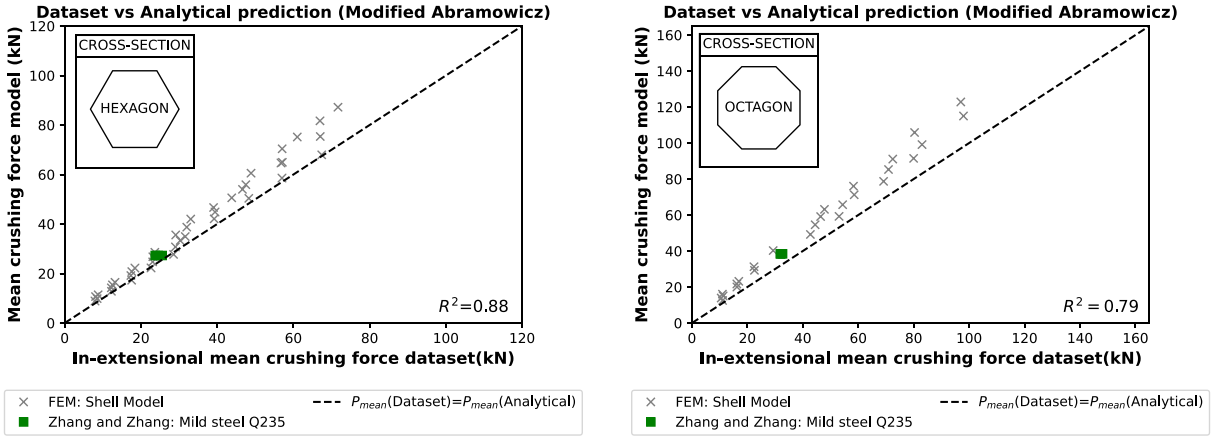

Fig. 15. (a) Comparison of model from Abramowicz et al. [10] (Modified) for hexagonal tubular structures; (b) Comparison of model from Abramowicz et al. [10] (Modified) for octagonal tubular structures.

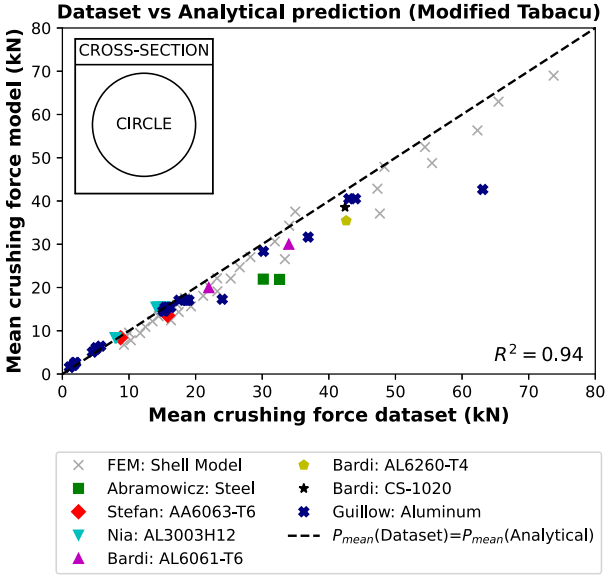

Fig. 16. Comparison of the modified Tabacu's model [2] for circular tubular structures.

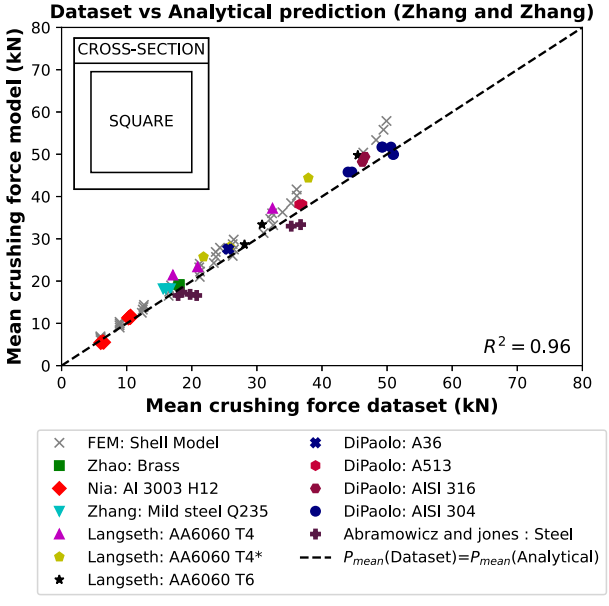

Fig. 17. Comparison of the Zhang and Zhang's model [2] for square tubular structures.

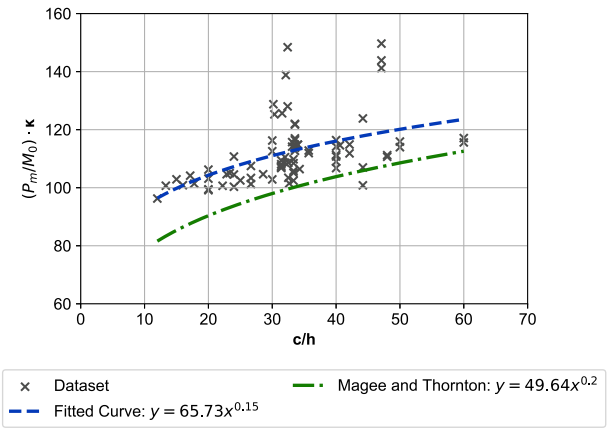

Fig. 18. Curve fit for our dataset using Eq. (60).

Table 1
Values of X, Y and Z for specific cases (Eq. (70))

S.No.	Case	X	Y	Z
1	Circular	33.85	0	0.5
2	Polygon (Extensional crushing mode)	12.56	0.5	0.5
3	Polygon (Inextensional crushing mode)	15.91	1.03	0.15

The term under the root can be rewritten as a function of N_c, since the central angle θ is a function of N_c. For $4 \leq N_c \leq 8$, the term under the root can be approximated very accurately (mean absolute percentage error = 0.23%) by a power law of the form $i.N_c^j$, where i and j are unknowns:

$$\sqrt{\frac{N_c^2 \cdot tan(\theta/2)}{(tan(\theta/2) + 0.06/tan(\theta/2))}} \approx 0.94 \cdot N_c^{1.03} \tag{68}$$

The final equation then takes a form similar to Eq. (64) and (65):

$$\frac{P_m}{M_0} \cdot \kappa = 15.91 \cdot N_c^{1.03} \cdot \left(\frac{c}{h}\right)^{0.15} \tag{69}$$

Based on Eqs. (64), (65) and (69), a general equation for mean crushing force of metallic tubular structures can be written in the form:

$$\frac{P_m}{M_0} \cdot \kappa = X \cdot N_c^Y \cdot \left(\frac{c}{h}\right)^Z \text{; c/h is replaced with R/h for circular tubular structures} \tag{70}$$

where, X, Y and Z vary based on the shape and crushing mode of the tubular structures. This form is especially interesting for preliminary design where various geometries and materials must be compared. The values of X,Y and Z for different cases have been presented in Table 1. A very good agreement between the analytical mean crushing force and the mean crushing dataset (comprising of all cross-sections and both the crushing modes) was obtained ($R^2 = 0.97$), the comparison is presented in Fig. 21.

12. Discussion

A summary indicating the average error of each model is provided in Table 2. Additionally, to better comprehend the distribution of errors throughout the entire dataset, the Inter-Quartile Range (IQR) is also given for all the models. IQR is a valuable measure in this context as it quantifies the spread of the middle 50% of the errors, providing insight into the reliability of these predictions. From Table 2, it can be noted that while the presented analytical models are a great way of quickly determining the mean crushing force, the spread of errors even for the best-fitting model is about 6%. Such models should therefore be used with caution, keeping the error ranges in mind.

For circular tubular structures, the model from Abramowicz et al. [9] was found to be the most accurate with a R^2 value of 0.98. The models from Weirzbicki et al. [11] and Singace et al. [12] were found to have similar accuracy (R^2 of 0.95 and 0.94 respectively). An underestimation ($\overline{E} = 26.4\%$) of the mean force is observed for the model from Alexander [8] which stems from the absence of an effective crushing length parameter. Similarly, the model from Tabacu et al. [9] also underestimates the mean crushing force, and the accuracy of the model is significantly improved when the fully plastic bending moment (M_0) is multiplied by $2/\sqrt{3}$, to account for the largely plain strain conditions.

For square tubular structures, the models from Magee and Thornton [25], and Abramowicz et al. [1] both show good agreement with experimental/numerical dataset. The model from Zhang and Zhang [15] calibrated to the model from Magee and Thronton (Eq. (58)) predicts the mean crushing force for polygonal tubular structures with R^2 value of 0.86 for hexagonal tubular structure and R^2 value of 0.9 for octagonal tubular structures. A calibration of Zhang and Zhang's model based on our dataset has also been proposed, which further improves the accuracy of Zhang and Zhang's model for polygonal tubular structures (R^2 (hexagonal) = 0.95 and R^2 (octagonal) = 0.97).

The quasi inextensional crushing model proposed by Abramowicz et al. for multicorner sheet metal columns (polygonal tubular structures) is found to overestimate the mean crushing force values by very large margins (hexagonal tubular structures: $\overline{E} = -53.5\%$ and octagonal tubular structures: $\overline{E} = -63.5\%$). The method attempts to model a mixed crushing mode using a timelike α and a switching point parameter $\overline{\alpha}$ by assuming that the crushing from $\alpha = 0$ to $\overline{\alpha}$ is inextensional while the crushing from $\overline{\alpha}$ to $\pi/2$ is extensional. Abramowicz's approach requires an accurate determination of the switching point parameter ($\overline{\alpha}$), which needs to be calculated alongside two other unknowns, namely: the radius of the torus b, and the crushing wavelength $2H$; and the model is very sensitive to slight changes of b or $2H$. In the present study, an attempt is made to correct the model by using the rate of change of area in place of the rate of plastic flow along the inclined hinge lines (Section 8). The equations obtained from the modified set of integrals provide a much more reasonable estimate of the mean crushing force compared to the original model, however, the model still overestimates the mean crushing force. (hexagonal tubular structures: $\overline{E} = -14.6\%$ and octagonal tubular structures: $\overline{E} = -25.3\%$)

For hexagonal and octagonal tubular structures, the results from Tabacu et al.'s model [2] are found to be quite accurate for extensional crushing (for hexagonal tubular structures: $R^2 = 0.99$ and for octagonal tubular structures: $R^2 = 0.93$). For inextensional crushing of hexagonal and octagonal tubular structures, Zhang and Zhang's model [15] calibrated to our dataset (Eq. (63)) predicted the mean crushing force with a better accuracy compared to other models ($R^2 = 0.95$ for hexagonal tubular structures and $R^2 = 0.97$ for octagonal tubular structures). The extensional crushing model from Tabacu et al. gives an R^2 of 0.86 for inextensional crushing of hexagonal tubular structures and 0.98 for inextensional crushing of octagonal tubular structures, reinforcing the observation made by Abramowicz et al. [10] that for quasi-inextensional crushing mode, the contribution of energy absorption due to extension is more dominant for obtuse angle elements.

Finally, a generalized equation (Eq. (70)) for axial crushing of tubular structures based on the models from Tabacu et al. (Eq. (30) and (55)) and Zhang and Zhang (Eq. (63)) is proposed which can be

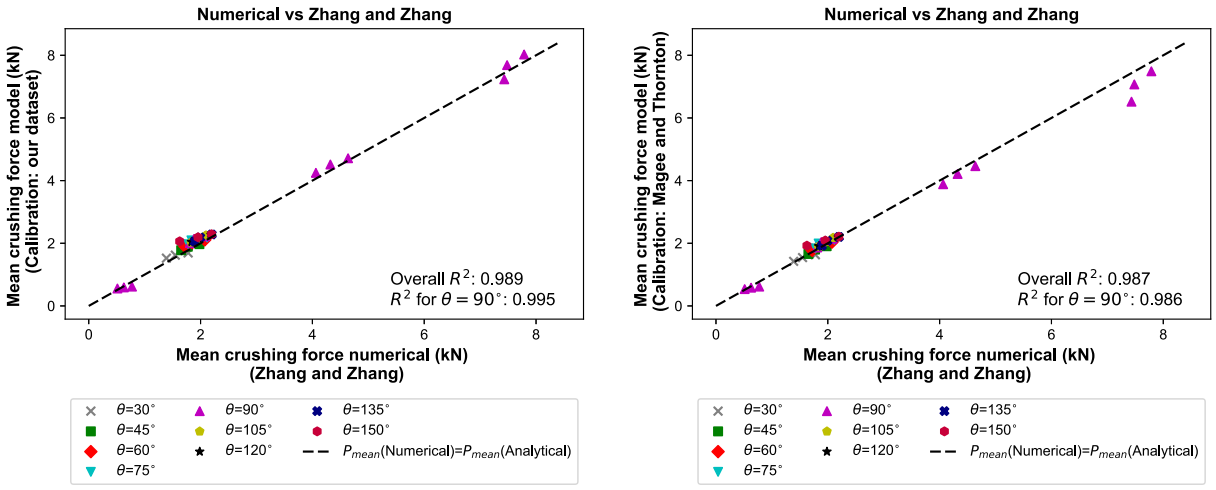

Fig. 19. Comparison of numerical (FEM results from Zhang and Zhang [15]) and analytical mean crushing force obtained using Zhang and Zhang's model calibrated with (a) Our dataset (b) Magee and Thornton's dataset.

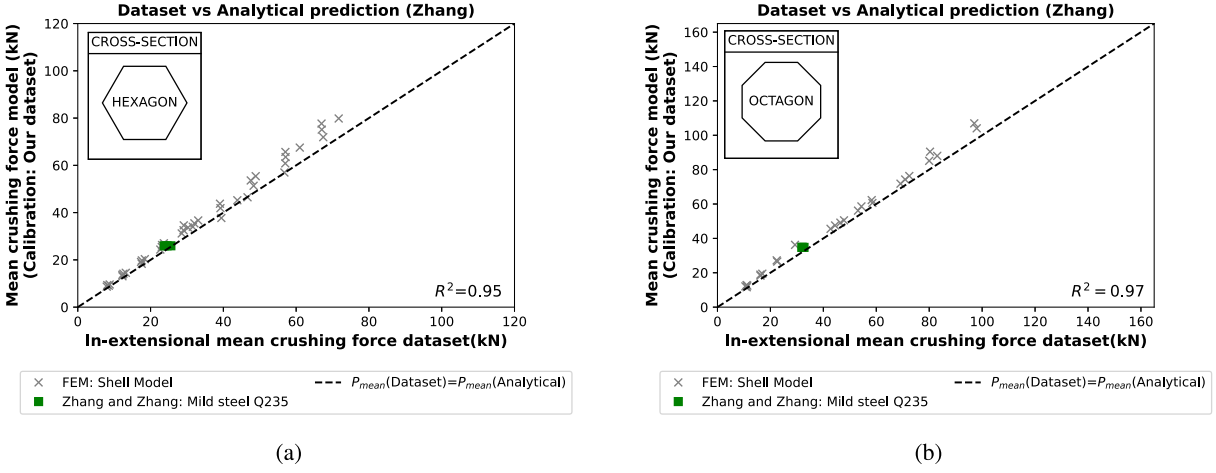

Fig. 20. Comparison of model from Zhang and Zhang [15] (calibrated with our dataset, Eq. (63)) for (a) hexagonal tubular structures and (b) octagonal tubular structures.

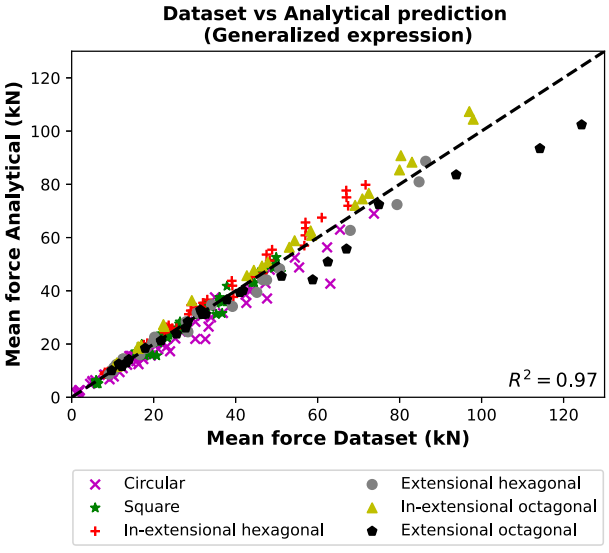

Fig. 21. Comparison between generalized expression for mean crushing force and mean crushing force dataset.

used to determine the mean crushing force for different cross-sectional shapes as well as crushing modes, demonstrating a high coefficient of determination (R^2) of 0.97, which underscores its predictive strength.

13. Conclusions

The purpose of this work was to identify and improve analytical models that can be employed to calculate the mean crushing force of metallic tubular structures, with the goal of reaching models that are fast and accurate to be applied in the preliminary design of structures taking crashworthiness into account. The existing and improved models were compared against experimental data from the literature, and numerical data generated with finite elements.

For circular tubular structures the model from Abramowicz et al. [9] demonstrates the best accuracy. The model from Tabacu et al. [2] in its original form consistently underestimates the P_{mean} for circular tubular structures. However, with the improvements herein proposed for circular tubular structures, the accuracy of the model is improved as evidenced by the improvement in the coefficient of determination (R^2) from 0.91 to 0.94, and a reduction in the average error ($\overline{E}$) from 9.9% to 3.5%. For inextensional crushing of square tubular structures, it is recommended to utilize the model proposed by Abramowicz et al. [1] (Eq. (17)) or the model proposed by Zhang and Zhang [15]

Table 2
Coefficient of determination (R^2), Average error ($\overline{E}$) and Interquartile range for various analytical models.

Model	Equation	R^2	$\overline{E}(\%)$	Interquartile range		
				Q_1	Q_3	Δ
Circular tubular structures						
Alexander	(12)	0.73	26.4	20.6	33.5	12.9
Abramowicz et al.	(13)	0.98	−4.9	−10.4	1.5	11.8
Wierzbicki et al.	(14)	0.95	3.9	−3.6	13.2	16.8
Singace et al.	(15)	0.94	6.5	1.3	13.3	11.9
Tabacu et al.	(29)	0.91	9.9	5	18	13.0
Modified Tabacu et al.	(55)	0.94	3.5	−0.9	12.2	13.1
Square tubular structures						
Magee and Thornton	(16)	0.95	8.4	4.5	12.8	8.4
Abramowicz et al.	(17)	0.95	−8.3	−14.2	−1.9	12.3
Tabacu et al.	(30)	0.59	−27.5	−37.8	−16.6	21.2
Hexagonal tubular structures (Inextensional)						
Abramowicz et al.	(19)	−0.29	−53.5	−63.2	−44.4	18.8
Abramowicz et al. (Mod.)	(49)	0.88	−14.6	−21.3	−8.7	12.6
Zhang and Zhang (Magee and Thornton)	(58)	0.86	−16.9	−20.5	−12.3	8.2
Zhang and Zhang (Our Calibration)	(63)	0.95	−9.3	−12.1	−6.7	5.4
Tabacu et al. (Extensional model)	(30)	0.86	−13.6	−22.6	−5.3	17.3
Hexagonal tubular structures (Extensional)						
Tabacu et al.	(30)	0.99	−0.9	−8.0	5.1	13.1
Octagonal tubular structures (Inextensional)						
Abramowicz et al.	(21)	−0.41	−63.5	−72.7	−55.3	17.4
Abramowicz et al. (Mod.)	(50)	0.79	−25.3	−31.8	−19.4	12.4
Zhang and Zhang (Magee and Thornton)	(58)	0.90	−32.5	−22.3	−13.8	8.5
Zhang and Zhang (Our Calibration)	(63)	0.97	−9.7	−12.6	−5.9	6.7
Tabacu et al. (Extensional model)	(30)	0.98	−4.3	−11.7	2.6	14.3
Octagonal tubular structures (Extensional)						
Tabacu et al.	(30)	0.93	5.8	1.9	10.8	8.9

(Eq. (59) and (63)). For inextensional crushing of polygonal tubular structures, the model from Zhang and Zhang calibrated to our dataset (Eq. (63)) for square tubular structures gives the best overall accuracy (R^2 (hexagonal) = 0.95 and R^2 (octagonal) = 0.97). And for extensional collapse of polygonal tubular structures, the model from Tabacu et al. [2] gives an R^2 of 0.99 for hexagonal tubular structures and an R^2 of 0.93 for octagonal tubular structures.

The model for quasi inextensional crushing of polygonal tubular structures from Abramowicz et al. [10], along with the models derived using Abramowicz et al.'s model (Maalej et al. [28], Liu and Day [13,14]), overestimated the mean crushing force by a large margin for both hexagonal and octagonal tubular structures ($\overline{E}$ (hexagon) = 53.5% and $\overline{E}$ (octagon) = 63.5%). An improvement was suggested to reduce the over-prediction, however, the model still overestimates the mean crushing force with an $\overline{E}$ of 14.6% for hexagonal tubular structures and 25.3% for octagonal tubular structures.

Based on the dataset of experimental results, we also observed that polygonal tubular structures with $N_c = 4$ have a tendency to crush in the inextensional crushing mode, while polygonal columns with $N_c \geq 8$ have a tendency to collapse in mixed or extensional collapse modes. It was also observed from the finite element results that as N_c approaches a value of 8, the tubular structures with $c/h \leq 30$ have a tendency to crush under extensional or mixed crushing mode, even when a type-I trigger (i.e. an inextensional trigger) is used. Therefore, for preliminary design, it can be considered that the crushing mode is inextensional for $N_c = 4$; however, for $N_c > 4$, both extensional and inextensional crushing modes need to be considered.

Based on the accuracy and similarity of some of these models (Eq. (55), (30) and (63)), a generalized form for the crushing of metallic tubular structures is also presented, which is shown to have a good accuracy for predicting the mean crushing force of circular and polygonal tubular structures ($R^2 = 0.97$).

The generalized model suggested for calculating the mean crushing force demonstrates high accuracy, evidenced by an R^2 value of 0.97. However, the coefficients applied for the inextensional crushing of polygonal tubular structures are derived from empirical calculations. Consequently, additional research is necessary to deepen the understanding of the inextensional crushing mechanism and enable the development of a mechanism-based approach for determining the mean crushing force for inextensional crushing of polygonal tubular structures.

CRediT authorship contribution statement

Shreyas Anand: Writing – original draft, Visualization, Validation, Methodology, Investigation, Formal analysis. **René Alderliesten:** Supervision, Resources. **Saullo G.P. Castro:** Writing – review & editing, Supervision, Resources, Project administration, Funding acquisition, Conceptualization.

Declaration of competing interest

The authors declare that they have no known competing financial interests or personal relationships that could have appeared to influence the work reported in this paper.

Data availability

Used data has been added to the manuscript as appendix and script files will be made available as a DOI.

Acknowledgments

The authors give special thanks to the Faculty of Aerospace Engineering of TU Delft for supporting this research, which is part of the Smart Flying-V project that addresses key technological challenges to enable unconventional aircraft configurations.

Appendix A. Experimental dataset from literature

A.1. Hexagonal tubular structures

S.No.	Reference	Material	c (mm)	h (mm)	P_m (kN)	$P_m(FEM)$ (kN)	Crushing mode
1	Zhang and Zhang [47]	Mild steel Q235	40	1.2	25.58	24.13	Inextensional
2			40	1.2	24.53	24.13	Inextensional
3			40	1.2	23.75	24.13	Inextensional
4	Fan et al. [20]	ASTM A36	33.2	1.5	46.6	48.84	Extensional
5	Liu et al. [48]	AA6061 - T4	15	1.2	10.2	12.78	Extensional
6	Nia and Hamedani [37]	Al 3003 H12	31.4	1.5	12.64	14.49	Extensional
7			31.4	1.5	12.62	14.49	Extensional
8			31.4	1.5	12.49	14.49	Extensional
9			31.4	1.5	12.5	14.49	Extensional

A.2. Octagonal tubular structures

S.No.	Reference	Material	c (mm)	h (mm)	P_m (kN)	$P_m(FEM)$ (kN)	Crushing mode
1	Zhang and Zhang [47]	Mild steel Q235	40	1.2	31.87	32.15	Mixed
2			40	1.2	32.09	32.15	Mixed
3			40	1.2	32.71	32.15	Mixed
4	Fan et al. [20]	ASTM A36	24.9	1.5	58.8	47.99	Extensional
5	Liu et al. [48]	AA6061 - T4	15	1.2	11.5	13.95	Extensional

A.3. Square tubular structures

S.No.	Reference	Material	c (mm)	h (mm)	P_m (kN)	$P_m(FEM)$ (kN)	Crushing mode
1	Zhao et al. [49]	Brass	35.00	1.50	18.00	21.08	Inextensional
2			35.00	1.50	18.09	21.08	Inextensional
3	Nia and Hamedani [37]	Al 3003 H12	47.10	1.50	10.50	10.84	Mixed
4			47.10	1.50	10.60	10.84	Extensional
5			47.10	1.50	10.40	10.84	Extensional
6			47.10	1.50	10.56	10.84	Mixed
7			47.10	1.50	10.27	10.84	Extensional
8			47.10	1.00	6.46	5.76	Inextensional
9			47.10	1.00	6.02	5.76	Inextensional
10			47.10	1.00	6.33	5.76	Inextensional
11	Zhang and Zhang [47]	Mild Steel Q235	40.00	1.20	16.01	16.08	Inextensional
12			40.00	1.20	16.72	16.08	Inextensional
13			40.00	1.20	15.60	16.08	Inextensional
14	Langseth et al. [22]	AA6060 T4	80.00	1.81	17.10	17.29	Inextensional
15			80.00	1.90	20.90	18.90	Inextensional
16			80.00	2.46	32.40	30.76	Inextensional
17		AA6060 T4*	80.00	1.81	21.80	22.50	Inextensional
18			80.00	1.90	25.80	24.29	Inextensional
19			80.00	2.45	37.90	36.54	Inextensional
20		AA6060 T6	80.00	1.81	28.10	25.81	Inextensional
21			80.00	1.97	30.80	28.19	Inextensional
22			80.00	2.46	45.50	39.98	Inextensional
23	DiPaolo and Tom [50]	A36	50.00	1.40	25.50	27.03	Inextensional
24			50.00	1.40	25.70	27.03	Inextensional
25		A513	50.00	1.51	36.50	34.58	Inextensional
26			50.00	1.51	37.00	34.58	Inextensional
27		AISI 316	50.00	1.47	46.20	44.29	Inextensional
28			50.00	1.47	46.20	44.29	Inextensional
29		AISI 304 - S2	50.00	1.49	36.60	45.05	Inextensional
30			50.00	1.49	44.60	39.94	Inextensional
31			50.00	1.49	44.00	39.94	Inextensional
32		AISI 304 - S3	50.00	1.49	50.90	44.12	Inextensional
33			50.00	1.49	51.00	44.12	Inextensional
34		AISI 304 - S4	50.00	1.49	50.60	45.31	Inextensional
35			50.00	1.49	49.30	45.31	Inextensional
36			50.00	1.49	49.20	45.31	Inextensional

S.No.	Reference	Material	c (mm)	h (mm)	P_m (kN)	$P_m(FEM)$ (kN)	Crushing mode
37	Abramo- wicz et al. [1]	Mild Steel	49.30	1.63	35.28	29.91	Inextensional
38			49.34	1.64	36.71	29.91	Inextensional
39			37.11	1.15	20.75	15.81	Extensional
40			37.11	1.15	17.90	15.81	Inextensional
41			37.10	1.16	19.75	15.46	Inextensional
42			37.06	1.18	18.50	15.72	Inextensional

A.4. Circular tubular structures

S.No.	Reference	Material	R (mm)	h (mm)	P_m (kN)	$P_m(FEM)$ (kN)	Crushing mode
1	Abramowi- cz et al. [9]	Mild Steel	27.94	1.20	32.60	–	c
2			28.10	1.20	30.16	–	c+d
3	Tabacu et al. [2]	AA6063 T6	20.00	1.23	15.80	16.36	c
4			19.50	0.90	8.74	10.07	d
5	Nia and Hamedani [37]	AL3003 H12	30.00	1.50	14.63	17.94	c+d
6			30.00	1.50	15.25	17.94	c+d
7			30.00	1.50	15.38	17.94	c+d
8			30.00	1.50	14.37	17.94	c+d
9			30.00	1.50	14.05	17.94	c+d
10			30.00	1.00	8.00	8.25	d
11			30.00	1.00	7.90	8.25	d
12			30.00	1.00	8.10	8.25	d
13	Bardi et al. [51]	AL6061 T6	15.28	1.26	21.97	19.67	c
14			15.08	1.66	33.99	32.31	c
15		AL6260 T4	28.94	2.04	42.61	–	c
16		CS 1020	15.31	1.26	42.43	–	c
17	Guillow et al. [52]	AA6060 T5	48.95	1.90	43.00	43.25	c
18			48.50	1.00	15.40	15.19	d
19			48.50	1.00	15.80	15.19	c+d
20			48.50	1.00	16.25	15.19	d
21			48.95	1.90	44.00	43.25	c+d
22			48.75	1.50	30.18	29.64	c+d
23			48.30	0.56	5.75	6.32	d
24			48.50	1.00	15.72	15.19	d
25			48.25	0.54	5.06	5.89	d
26			48.15	0.26	1.66	1.50	d
27			48.10	0.22	1.10	1.17	d
28			48.15	0.31	1.84	2.12	d
29			48.15	0.29	1.83	1.88	d
30			48.15	0.31	2.00	2.12	d
31			48.25	0.52	5.06	5.30	d
32			24.20	1.35	18.70	19.42	c+d
33			24.20	1.35	17.50	19.42	c
34			24.20	1.35	19.00	19.42	c+d
35			24.20	1.35	18.50	19.42	c+d
36			24.15	1.35	18.75	19.24	c
37			15.20	1.59	24.00	17.14	c
38			14.50	2.95	63.10	–	c
39			28.95	1.92	36.90	32.33	c
40			28.25	0.57	4.50	5.12	d
41			28.55	1.15	15.33	15.87	c+d
42			28.55	1.15	15.10	15.87	d
43			28.05	0.31	1.64	1.88	d
44			48.10	0.22	1.07	1.17	d

c = concertina crushing mode ; d = diamond crushing mode

Appendix B. Material data

Note: In most instances, the value of flow stress is obtained using Eq. (6), except when required data is unavailable. It is also important to note that stainless steel tubular structures (AISI-304 and AISI-316) can undergo martensitic transformation resulting in a change of material properties [50]. We found that the flow stress values obtained using Eq. (5) provide much better estimations of the mean crushing force for such cases.

S.No.	Material	Reference	σ_y (MPa)	σ_u (MPa)	σ_0: [Eq. (6)] (MPa)	σ_0: [Eq. (5)] (MPa)
1	Brass	Zhao et al. [49]	173.0	367.5	291.5	270.3
2	AL3003 H12	Nia and Hamedani. [37]	130.0	137.8	136.4	133.9
3	Mild Steel Q235	Zhang and Zhang [47]	218.5	323.3	305.5	270.9
4	AA6060 T4	Langseth et al. [22]	76.3	165.3	150.3	120.8
5	AA6060 T4*		133.3	200.3	184.6	166.8
6	AA6060 T6		188.3	212.0	205.5	200.2
7	A36	DiPaolo and Tom [50]	340.0	364.0	358.0	352.0
8	A513		400.0	448.0	431.9	424.0
9	AISI316		468.0	679.0	637.2	573.5
10	AISI304 -S2		380.0	683.0	598.1	531.5
11	AISI304 -S3		420.0	740.0	659.9	580.0
12	AISI304 -S4		439.0	761.0	677.1	600.0
13	Mild Steel	Abramowicz et al. [1]	264.5	328.5	311.4	296.5
14	Steel	Abramowicz et al. [9]	222	336	–	279
15	AA6063 T6	Tabacu et al. [2]	170	222	197	196
16	AL6061 T6	Bardi et al. [51]	300.8	–	320.1	–
17	AL6260 T4		128	–	200.4	–
18	CS 1020		537.9	–	617.6	–
19	Aluminum	Guillow et al. [52]	180	212.5	199.1	196.3
20	ASTM A36	Fan et al. [20]	265	425.8	379.7	345.4
21	AA6061 T4	Liu et al. [48]	112.4	214.2	193.7	163.3

Appendix C. Numerical dataset

C.1. Square and circular tubular structures

S.No.	2R or c (mm)	h (mm)	P_{mean} (kN)			
			Circular		Square (Inextensional)	
			AA6060 T4	AISI 316	AA6060 T4	AISI 316
1	30	1	9.24	33.40	6.00	23.40
2	30	1.25	11.68	47.66	8.90	33.90
3	30	1.5	16.30	55.49	12.30	46.30
4	30	1.75	19.31	–	16.40	–
5	30	2	23.26	–	21.20	–
6	30	2.25	–	–	26.30	–
7	30	2.5	–	–	31.00	–
8	40	1	10.27	31.89	6.00	23.70
9	40	1.25	12.45	47.29	8.90	35.20
10	40	1.5	17.47	62.31	12.50	48.30
11	40	1.75	21.14	–	16.50	–
12	40	2	25.27	–	21.30	–
13	40	2.25	–	–	26.50	–
14	40	2.5	–	–	32.50	–
15	50	1	9.63	34.04	6.00	23.70
16	50	1.25	13.53	48.34	8.90	36.10
17	50	1.5	17.24	65.47	12.60	49.50
18	50	1.75	22.05	–	16.50	–
19	50	2	26.62	–	21.10	–
20	50	2.25	–	–	26.30	–
21	50	2.5	–	–	32.10	–
22	60	1	9.99	34.95	6.00	24.30
23	60	1.25	14.44	54.43	8.90	36.10
24	60	1.5	18.39	73.74	12.60	49.90
25	60	1.75	23.22	–	16.80	–
26	60	2	28.23	–	21.20	–
27	60	2.25	–	–	26.40	–
28	60	2.5	–	–	32.30	–

Geometrical parameters:
$2R$ = diameter of circular tubular structures
c = edge length of square tubular structures
h = wall thickness
Material parameters:
AA6060 T4: $\kappa = 0.73$, $\sigma_y = 76$ MPa, $\sigma_u = 165$ MPa and $\sigma_0 = 151$ MPa
AISI 316 : $\kappa = 0.77$, $\sigma_y = 467$ MPa, $\sigma_u = 678$ MPa and $\sigma_0 = 624$ MPa

C.2. Hexagonal and octagonal tubular structures (inextensional)

S.No.	c (mm)	h (mm)	P_{mean} (kN)			
			Hexagonal		Octagonal	
			AA6060 T4	AISI 316	AA6060 T4	AISI 316
1	30	1	7.96	31.63	11.08	42.74
2	30	1.12	–	39.21	–	53.09
3	30	1.25	12.27	48.31	–	–
4	30	1.37	–	57.00	–	–
5	30	1.5	17.57	67.44	–	–
6	30	1.75	22.66	–	–	–
7	30	2	28.57	–	–	–
8	40	1	8.52	32.03	10.55	44.44
9	40	1.12	–	39.07	–	54.39
10	40	1.25	12.24	47.54	16.25	69.15
11	40	1.37	–	57.11	–	79.98
12	40	1.5	17.37	67.05	–	–
13	40	1.75	23.09	–	–	–
14	40	2	29.05	–	–	–
15	50	1	8.09	33.08	11.26	46.43
16	50	1.12	–	43.83	–	58.54
17	50	1.25	12.52	48.89	16.22	70.92
18	50	1.37	–	57.04	–	83.02
19	50	1.5	17.61	66.98	22.56	97.97
20	50	1.75	23.13	–	–	–
21	50	2	30.29	–	–	–
22	60	1	8.77	39.45	11.01	47.81
23	60	1.12	–	46.64	–	58.29
24	60	1.25	13.20	56.76	16.93	72.47
25	60	1.37	–	61.01	–	80.32
26	60	1.5	18.43	71.70	22.39	97.01
27	60	1.75	23.66	–	29.31	–
28	60	2	29.13	–	–	–

Note: The parameters and material data are the same as Appendix C.1

C.3. Hexagonal and octagonal tubular structures (extensional)

S.No.	c (mm)	h (mm)	P_{mean} (kN)			
			Hexagonal		Octagonal	
			AA6060 T4	AISI 316	AA6060 T4	AISI 316
1	30	1	9.11	39.22	9.75	41.05
2	30	1.5	16.63	67.97	17.95	74.95
3	30	2	28.36	–	28.35	–
4	40	1	10.19	45.18	12.27	51.20
5	40	1.5	18.13	79.36	21.80	93.80
6	40	2	27.91	–	31.41	–
7	50	1	10.34	47.56	13.36	62.49
8	50	1.5	19.75	84.75	25.62	114.23
9	50	2	30.59	–	37.86	–
10	60	1	10.89	50.73	13.96	67.03
11	60	1.5	20.21	86.36	27.81	124.4
12	60	2	34.10	–	41.78	–

Note: The parameters and material data are the same as Appendix C.1

References

[1] Abramowicz Wlodzimierz, Jones Norman. Dynamic axial crushing of square tubes. Int J Impact Eng 1984;2:179–208. http://dx.doi.org/10.1016/0734-743X(84)90005-8.

[2] Tabacu Stefan, Ducu Cătălin. An analytical solution for the estimate of the mean crushing force of structures with polygonal and star-shaped cross-sections subjected to axial load. Int J Mech Sci 2019;161–162:105010. http://dx.doi.org/10.1016/J.IJMECSCI.2019.105010.

[3] Ritchie Hannah, Roser Max, Rosado Pablo. CO_2 and greenhouse gas emissions (revision August 2020). Our World Data 2020. URL https://ourworldindata.org/co2-and-greenhouse-gas-emissions.

[4] IATA. Net zero resolution fact sheet. International Air Transport Association (IATA); 2022, URL https://www.iata.org/en/iata-repository/pressroom/fact-sheets/fact-sheet----iata-net-zero-resolution/.

[5] EIA. International energy outlook 2021. US Energy Information Administration; 2021, URL www.eia.gov/outlooks/ieo/.

[6] Oosterom Wilco, Vos Roelof. Conceptual design of a flying-V aircraft family. In: AIAA AVIATION 2022 forum. American Institute of Aeronautics and Astronautics; 2022, http://dx.doi.org/10.2514/6.2022-3200.

[7] Airbus A350 aircraft characteristics airport and maintenance planning AC. Airbus S.A.S; 2021, URL https://www.airbus.com/sites/g/files/jlcbta136/files/2021-11/Airbus-Commercial-Aircraft-AC-A350-900-1000.pdf.

[8] Alexander JM. An approximate analysis of the collapse of thin cylindrical shells under axial loading. Quart J Mech Appl Math 1960;13:10–5. http://dx.doi.org/10.1093/QJMAM/13.1.10, URL https://academic.oup.com/qjmam/article/13/1/10/1919943.

[9] Abramowicz Wlodzimierz, Jones Norman. Dynamic axial crushing of circular tubes. Int J Impact Eng 1984;2:263–81. http://dx.doi.org/10.1016/0734-743X(84)90010-1.

[10] Abramowicz W, Wierzbicki T. Axial crushing of multicorner sheet metal columns. J Appl Mech 1989;56:113–20. http://dx.doi.org/10.1115/1.3176030.

[11] Wierzbicki T, Bhat SU, Abramowicz W, Brodkin D. Alexander revisited—A two folding elements model of progressive crushing of tubes. Int J Solids Struct 1992;29:3269–88. http://dx.doi.org/10.1016/0020-7683(92)90040-Z.

[12] Singace AA, Elsobky H, Reddy TY. On the eccentricity factor in the progressive crushing of tubes. Int J Solids Struct 1995;32:3589–602. http://dx.doi.org/10.1016/0020-7683(95)00020-B.

[13] Liu Y, Day ML. Development of simplified finite element models for straight thin-walled tubes with octagonal cross section. Int J Crashworthiness 2007;12(5):503–8. http://dx.doi.org/10.1080/13588260701483557.

[14] Liu Yucheng, Day Michael L. Axial crushing of thin-walled columns with octagonal section: Modeling and design. In: Ao Sio-Iong, Rieger Burghard, Chen Su-Shing, editors. Advances in computational algorithms and data analysis. Dordrecht: Springer Netherlands; 2009, p. 365–79. http://dx.doi.org/10.1007/978-1-4020-8919-0_25.

[15] Zhang Xiong, Zhang Hui. Theoretical and numerical investigation on the crush resistance of rhombic and kagome honeycombs. Compos Struct 2013;96:143–52. http://dx.doi.org/10.1016/j.compstruct.2012.09.028, URL https://www.sciencedirect.com/science/article/pii/S0263822312004679.

[16] Zhang Xiong, Zhang Hui. Axial crushing of circular multi-cell columns. Int J Impact Eng 2014;65:110–25. http://dx.doi.org/10.1016/J.IJIMPENG.2013.12.002.

[17] Mamalis AG, Manolakos DE, Ioannidis MB, Kostazos PK, Dimitriou C. Finite element simulation of the axial collapse of metallic thin-walled tubes with octagonal cross-section. Thin-Walled Struct 2003;41:891–900. http://dx.doi.org/10.1016/S0263-8231(03)00046-6.

[18] Tarlochan F, Samer F, Hamouda AMS, Ramesh S, Khalid Karam. Design of thin wall structures for energy absorption applications: Enhancement of crashworthiness due to axial and oblique impact forces. Thin-Walled Struct 2013;71:7–17. http://dx.doi.org/10.1016/J.TWS.2013.04.003.

[19] Yamashita Minoru, Gotoh Manabu, Sawairi Yasuhiko. Axial crush of hollow cylindrical structures with various polygonal cross-sections: Numerical simulation and experiment. J Mater Process Technol 2003;140:59–64. http://dx.doi.org/10.1016/S0924-0136(03)00821-5.

[20] Fan Z, Lu G, Liu K. Quasi-static axial compression of thin-walled tubes with different cross-sectional shapes. Eng Struct 2013;55:80–9. http://dx.doi.org/10.1016/J.ENGSTRUCT.2011.09.020.

[21] Wierzbicki Tomasz. Crushing analysis of metal honeycombs. Int J Impact Eng 1983;1:157–74. http://dx.doi.org/10.1016/0734-743X(83)90004-0.

[22] Langseth M, Hopperstad OS. Static and dynamic axial crushing of square thin-walled aluminium extrusions. Int J Impact Eng 1996;18:949–68. http://dx.doi.org/10.1016/S0734-743X(96)00025-5.

[23] Hanssen AG, Langseth M, Hopperstad OS. Static crushing of square aluminium extrusions with aluminium foam filler. Int J Mech Sci 1999;41:967–93. http://dx.doi.org/10.1016/S0020-7403(98)00064-2.

[24] Yang PDC, Caldwell JB. Collision energy absorption of ships' bow structures. Int J Impact Eng 1988;7:181–96. http://dx.doi.org/10.1016/0734-743X(88)90025-5.

[25] Magee CL, Thornton PH. Design considerations in energy absorption by structural collapse. SAE Trans 1978;2041–55, URL https://web.mit.edu/cmagee/www/documents/07-magee_thornton-energy_absorption_structural_collapse_SAE_1978.pdf.

[26] Abramowicz W, Wierzbicki T. Axial crushing of foam-filled columns. Int J Mech Sci 1988;30:263–71. http://dx.doi.org/10.1016/0020-7403(88)90059-8.

[27] Wierzbicki Tomasz, Huang Joan. Initiation of plastic folding mechanism in crushed box columns. Thin-Walled Struct 1992;13:115–43. http://dx.doi.org/10.1016/0263-8231(92)90005-H.

[28] Maalej Yamen, Chaari Fahmi, Zouari Bassem, Markiewicz Eric. Closed form solution for the collapse of polygonal thin-walled columns in the axial crushing case. J Theoret Appl Mech 2014;52:707–18, URL http://jtam.pl/pdf-102150-33710?filename=Closed%20form%20solution%20for.pdf.

[29] Ohkubo Y, Akamatsu T, Shirasawa K. Mean crushing strength of closed-hat section members. SAE Trans 1974;83:223–32, ISSN: 0096-736X, 2577-1531. URL http://www.jstor.org/stable/44721384.

[30] Wimmer A. Einfluss der Belastungsgeschwindigheit auf das Festigkeitsund Verformungsverhaten von Blechkonstruktionen am Beispiel von Kraftfahrzengen. ATZ 1975;77:281–6.

[31] Akerstrom Ture, Wierzbicki Tomaz. Dynamic crushing of strain rate sensitive box columns. In: 2nd international conference on vehicle structural mechanics. SAE International; 1977, http://dx.doi.org/10.4271/770592.

[32] Wierzbicki T, Abramowicz W. Crushing of thin-walled strain rate sensitive structures. Rozpr Inzynierskie 1981;29(1):153–63, URL https://www.scopus.com/inward/record.uri?eid=2-s2.0-0019651247&partnerID=40&md5=88feb31ce3434472bf2f5be919b0da0d.

[33] Jones Norman. Dynamic progressive buckling. In: Structural impact. Cambridge University Press; 1990, p. 385–431. http://dx.doi.org/10.1017/CBO9780511624285.010.

[34] Fauziah Mat, Azwan Ismail Khairul, Masniezam Ahmad, Sazali Yaacob, Othman Inayatullah. Dynamic axial crushing of empty and foam-filled conical aluminium tubes: Experimental and numerical analysis. Appl Mech Mater 2014;566:305–9. http://dx.doi.org/10.4028/WWW.SCIENTIFIC.NET/AMM.566.305, URL https://www.scientific.net/AMM.566.305.

[35] Malawat Mohammad, Sumarsono Danardono Agus, Istiyanto Jos, Prayogo Gatot, Dionisius Felix. Theoretical prediction of dynamic axial crushing on a square tube with eight holes used as a crush initiator. Int J Technol 2019;10:1042–55. http://dx.doi.org/10.14716/IJTECH.V10I5.2297, URL https://ijtech.eng.ui.ac.id/article/view/2297.

[36] Anand Shreyas, Alderliesten René, Castro Saullo GP. Dataset for crashworthiness in preliminary design: mean crushing force prediction for closed-section thin-walled metallic structures. Zenodo; 2024, http://dx.doi.org/10.5281/zenodo.10522974.

[37] Nia Ali Alavi, Hamedani Jamal Haddad. Comparative analysis of energy absorption and deformations of thin walled tubes with various section geometries. Thin-Walled Struct 2010;48:946–54. http://dx.doi.org/10.1016/J.TWS.2010.07.003.

[38] Zhang Xiong, Huh Hoon. Crushing analysis of polygonal columns and angle elements. Int J Impact Eng 2010;37:441–51. http://dx.doi.org/10.1016/j.ijimpeng.2009.06.009, URL https://www.sciencedirect.com/science/article/pii/S0734743X09001225.

[39] Abaqus/CAE user's guide. In: SIMULIA user assistance 2021. Dassault Systemes, URL https://help.3ds.com/2021/English/DSSIMULIA_Established/SIMACAECAERefMap/simacae-c-ov.htm?contextscope=all&id=7d6038c876dd40b984c8f7cd798ba0b8.

[40] Siva Kumar A. Experimental investigations with crush box simulations for different segment cars using LS-DYNA. Int J Curr Eng Technol 2013;2:670–6. http://dx.doi.org/10.14741/IJCET/SPL.2.2014.127.

[41] Harhash Mohamed, Kuhtz Moritz, Richter Jonas, Hornig Andreas, Gude Maik, Palkowski Heinz. Trigger geometry influencing the failure modes in steel/polymer/steel sandwich crashboxes: Experimental and numerical evaluation. Compos Struct 2021;262:113619. http://dx.doi.org/10.1016/J.COMPSTRUCT.2021.113619.

[42] Shanahan Dennis F. Human tolerance and crash survivability. RTO-EN-HFM-113, NATO; 2004, URL https://www.sto.nato.int/publications/STO%20Educational%20Notes/RTO-EN-HFM-113/EN-HFM-113-06.pdf.

[43] Yang Xianfeng, Ma Jingxuan, Wen Dongsheng, Yang Jialing. Crashworthy design and energy absorption mechanisms for helicopter structures: A systematic literature review. Prog Aerosp Sci 2020;114:100618. http://dx.doi.org/10.1016/J.PAEROSCI.2020.100618.

[44] Airoldi Alessandro, Janszen Gerardus. A design solution for a crashworthy landing gear with a new triggering mechanism for the plastic collapse of metallic tubes. Aerosp Sci Technol 2005;9:445–55. http://dx.doi.org/10.1016/J.AST.2005.04.001.

[45] Abramowicz W, Jones N. Dynamic progressive buckling of circular and square tubes. Int J Impact Eng 1986;4:243–70. http://dx.doi.org/10.1016/0734-743X(86)90017-5.

[46] Wierzbicki T, Abramowicz W. On the crushing mechanics of thin-walled structures. J Appl Mech 1983;50:727–34. http://dx.doi.org/10.1115/1.3167137.

[47] Zhang Xiong, Zhang Hui. Experimental and numerical investigation on crush resistance of polygonal columns and angle elements. Thin-Walled Struct 2012;57:25–36. http://dx.doi.org/10.1016/J.TWS.2012.04.006.

[48] Liu Wangyu, Lin Zhenqiong, Wang Ningling, Deng Xiaolin. Dynamic performances of thin-walled tubes with star-shaped cross section under axial impact. Thin-Walled Struct 2016;100:25–37. http://dx.doi.org/10.1016/J.TWS.2015.11.016.

[49] Zhao Han, Abdennadher Salim, Othman Ramzi. An experimental study of square tube crushing under impact loading using a modified large scale SHPB. Int J Impact Eng 2006;32(7):1174–89. http://dx.doi.org/10.1016/j.ijimpeng.2004.09.013, URL https://www.sciencedirect.com/science/article/pii/S0734743X04001952.

[50] DiPaolo BP, Tom JG. A study on an axial crush configuration response of thin-wall, steel box components: The quasi-static experiments. Int J Solids Struct 2006;43:7752–75. http://dx.doi.org/10.1016/J.IJSOLSTR.2006.03.028.

[51] Bardi FC, Yun HD, Kyriakides S. On the axisymmetric progressive crushing of circular tubes under axial compression. Int J Solids Struct 2003;40:3137–55. http://dx.doi.org/10.1016/S0020-7683(03)00111-2.

[52] Guillow SR, Lu G, Grzebieta RH. Quasi-static axial compression of thin-walled circular aluminium tubes. Int J Mech Sci 2001;43:2103–23. http://dx.doi.org/10.1016/S0020-7403(01)00031-5.